Available at
www.ElsevierMathematics.com
POWERED BY SCIENCE DIRECT

ELSEVIER Journal of Computational and Applied Mathematics 164–165 (2004) 53–80

JOURNAL OF COMPUTATIONAL AND APPLIED MATHEMATICS

www.elsevier.com/locate/cam

Central schemes and systems of conservation laws with discontinuous coefficients modeling gravity separation of polydisperse suspensions

S. Berres[a,*], R. Bürger[a], K.H. Karlsen[b]

[a] *Institute of Applied Analysis and Numerical Simulation, University of Stuttgart, Pfaffenwaldring 57, D-70569 Stuttgart, Germany*

[b] *Department of Mathematics, University of Bergen, Johs. Brunsgt. 12, N-5008 Bergen, Norway*

Received 15 September 2002; received in revised form 26 February 2003

Abstract

In this paper, two existing one-dimensional mathematical models, one for continuous sedimentation of monodisperse suspensions and one for settling of polydisperse suspensions, are combined into a model of continuous separation of polydisperse mixtures. This model can be written as a first-order system of conservation laws for the local concentrations of each particle species with a flux vector that depends discontinuously on the space variable. This application motivates the extension of the Kurganov–Tadmor central difference scheme to systems with discontinuous flux. The new central schemes are based on discretizing an enlarged system in which the discontinuous coefficients are viewed as additional conservation laws. These additional conservation laws can either be discretized and the evolution of the discontinuity parameters is calculated in each time step, or solved exactly, that is, the discontinuity parameters are kept constant (with respect to time). Numerical examples and an L^1 error study show that the Kurganov–Tadmor scheme with first-order in time discretization produces spurious oscillations, whereas its semi-discrete version, discretized by a second-order Runge–Kutta scheme, produces good results. The scheme with discontinuity parameters kept constant is slightly more accurate than when these are evolved. Numerical examples illustrate the application to separation of polydisperse suspensions.

Keywords: Polydisperse suspension; Sedimentation; Conservation law; Hyperbolic-elliptic system; Central difference scheme; Numerical simulation

* Corresponding author.

E-mail addresses: berres@mathematik.uni-stuttgart.de (S. Berres), buerger@mathematik.uni-stuttgart.de (R. Bürger), kennethk@mi.uib.no (K.H. Karlsen).

URLs: http://www.mathematik.uni-stuttgart.de/ians/LstAngMath/Berres/, http://www.mathematik.uni-stuttgart.de/ians/LstAngMath/Buerger/, http://www.mi.uib.no/kennethk/

0377-0427/$ - see front matter © 2003 Elsevier B.V. All rights reserved.
doi:10.1016/S0377-0427(03)00496-5

1. Introduction

In this paper we seek "easy to implement" numerical schemes for $N \times N$ systems of conservation laws with a flux vector containing discontinuous coefficients:

$$\partial_t \Phi + \partial_x \mathbf{f}(\gamma(x), \Phi) = 0, \tag{1.1}$$

where $\Phi := (\phi_1, \ldots, \phi_N)^{\mathrm{T}}$ is the unknown state vector and $\mathbf{f} := (f_1, \ldots, f_N)^{\mathrm{T}}$ is a given flux vector, which depends on the space variable x through the vector-valued parameter

$$\gamma(x) = (\gamma^1(x), \ldots, \gamma^p(x)).$$

The basic assumption is that the spatially varying coefficient γ is of bounded total variation. In applications, γ is typically piecewise smooth with finitely many jump discontinuities, or even piecewise constant with finitely many jumps. Our interest in such problems is motivated from models of continuous sedimentation of polydisperse suspensions of small spheres of N classes which differ in size or density. Such models are of widespread use in mineral processing, chemical engineering, volcanology and medicine.

In recent years there has been a lot of interest in conservation laws (and related equations) with discontinuous coefficients in many applications including flow in porous media [28,43,70], sedimentation processes (relevant references are provided below), and traffic flow on a highway [31,55]. They also arise in radar shape-from-shading problems [61,62] as well as other related Hamilton-Jacobi equations [63], see also [36]. Other applications are blood flow after endovascular repair [18], gas flow in variable duct [50], and conservation laws with source term [30,34].

The usual way to cope with the discontinuous parameter $\gamma(x)$ is to express it as an additional conservation law (see, e.g., [27,33])

$$\partial_t \gamma(x) = 0, \tag{1.2}$$

so that we arrive at the following enlarged $(N + p) \times (N + p)$ system of conservation laws

$$\partial_t \mathbf{u} + \partial_x \mathbf{F}(\mathbf{u}) = 0, \tag{1.3}$$

where $\mathbf{u} = (\phi_1, \ldots, \phi_N, \gamma_1, \ldots, \gamma_p)^{\mathrm{T}}$ and $\mathbf{F} = (f_1, \ldots, f_N, 0, \ldots, 0)^{\mathrm{T}}$. Note that (1.2) introduces linearly degenerate fields in the system (1.2) with eigenvalues that are zero. Consequently, if the eigenvalues of the Jacobian of the system (1.1) (for fixed γ) include eigenvalues that are zero (this is case with the systems that are considered in this paper), then the system (1.3) is nonstrictly hyperbolic and experiences so-called nonlinear resonant behavior, which implies that wave interactions are much more complicated than in strictly hyperbolic systems. In fact, one cannot expect to bound the total variation of the conserved quantities directly, but only when measured under a certain singular mapping, as was done first in [70] for approximate solutions generated by the Glimm scheme. This of course causes both mathematical and numerical difficulties as standard ideas and theory cannot be applied. Although some results of mathematical and numerical analysis exist for general systems like (1.3), see [32,33], it is the "scalar case", i.e., $p = 1$ and $N = 1$ (i.e., (1.3) becomes a 2×2 system) that has been most investigated in the literature. It is outside the scope of this paper to give a detailed overview of the existing literature, but let us mention that convergence with the singular mapping approach has been established for the 2×2 Godunov method in [33,48,49] and for 2×2 front tracking methods [28,41–43]. Convergence for the scalar Engquist-Osher and Godunov

schemes has been proved in [71,72], again using the singular mapping approach. Extensions of this scalar convergence analysis to degenerate parabolic equations with discontinuous coefficients can be found in [39]. Scalar relaxation schemes are analyzed in [35], while convergence of the vanishing viscosity/smoothing method is proved in [38]. The papers [35,38] use the compensated compactness method for the convergence analysis, while all the other papers cited use the singular mapping approach. Regarding uniqueness in the scalar case, see [37,41–43,67,71]. Some other numerical schemes without a theoretical foundation can be found in [2,67].

For the particular model that is studied in this paper when $N = 1$ (and $p = 2$), a 2×2 front tracking scheme is analyzed in [10], a scalar finite difference scheme is analyzed in [15] (see also [12]), while a relaxation scheme is analyzed in [11]. Moreover, a complete well-posedness (existence and uniqueness) theory in a certain functional class is given in [15]. We mention that for $N > 1$, there exist no results of mathematical and numerical analysis.

Although we are here interested in nonlinear equations with discontinuous coefficients, we still refer to [7,29,65] for an analysis of linear transport equations with discontinuous coefficients.

The present paper has two goals. Firstly, we formulate a model of continuous separation of polydisperse suspensions of rigid spheres as a straightforward combination of existing models on the one hand, of continuous sedimentation of monodisperse suspensions and on the other hand, of batch settling of polydisperse suspensions. The resulting model is expressed as a system of conservation laws with discontinuous flux (1.1). If particles with different densities are involved, then complex eigenvalues of the Jacobian of the flux-density vector may occur. In this case, the system is of mixed hyperbolic-elliptic ($N = 2$) or nonhyperbolic ($N \geqslant 3$) type.

Secondly, we use this model as an example to demonstrate that the second-order central scheme in [44] (briefly, the KT scheme) can be applied to solve numerically systems like (1.1). In fact, we demonstrate that it is possible to extend the KT scheme to systems of conservation laws with a discontinuous flux in several straightforward ways, based on the enlarged system (1.3). Several variants are compared by an application to a scalar sample problem, including an L^1 error study. The best performing scheme is applied to simulate continuous separation of bidisperse suspensions utilizing published experimental data.

The remaining part of this paper is organized as follows: In Section 2 the mathematical model is derived in detail. Section 3 is devoted to deriving the numerical schemes, while numerical experiments are presented and discussed in Section 4. Concluding remarks are given in Section 5.

2. Mathematical model of polydisperse gravity separation

2.1. Multidimensional model equations

We consider a polydisperse suspension of rigid particles, for simplicity assumed to be of spherical shape, which are dispersed in a viscous fluid of density ϱ_f and of dynamic viscosity μ_f. The solid particles belong to N different species having size (diameter) d_i and density ϱ_i, $i = 1, \ldots, N$, where we assume that the species are distinguishable, i.e. $d_i \neq d_j$ or $\varrho_i \neq \varrho_j$ for $i \neq j$. To be consistent with previous treatments we assume here $d_1 \geqslant d_2 \geqslant \cdots \geqslant d_N$. A set of generic model equations for the three-dimensional motion of the mixture was derived in [16] by starting from the mass and linear momentum balances for the fluid and each solid species considered as a separate phase, introducing

constitutive assumptions and simplifying the model equations as a consequence of a dimensional analysis. Details of the derivation have been included into a series of papers [5,6,9,16,17] and are therefore omitted here.

The resulting model equations can be written as

$$\partial_t \phi_i + \nabla \cdot (\phi_i \mathbf{q} + f_i(\Phi)\mathbf{k}) = 0, \quad i = 1, \ldots, N, \tag{2.1}$$

$$\nabla \cdot \mathbf{q} = 0, \tag{2.2}$$

$$\nabla p = -\varrho(\Phi) g \mathbf{k} + \frac{1}{1-\phi} \nabla \cdot \mathbf{T}_{\mathrm{f}}^{\mathrm{E}}. \tag{2.3}$$

Here ϕ_i is the local solids concentration of Species i (having diameter d_i and density ϱ_i), t is time, $\mathbf{q}$ is the volume average flow velocity of the mixture, $\Phi := (\phi_1, \ldots, \phi_N)^{\mathrm{T}}$ is the vector of the solids concentrations, $\mathbf{f}(\Phi) := (f_1(\Phi), \ldots, f_N(\Phi))^{\mathrm{T}}$ is the flux density vector (with given functions f_i to be discussed below), and $\mathbf{k}$ is the upwards pointing unit vector. In Eq. (2.3) p denotes the pore pressure, $\varrho(\Phi) := \varrho_1 \phi_1 + \cdots + \varrho_N \phi_N + (1-\phi)\varrho_{\mathrm{f}}$ is the local density of the mixture, g is the acceleration of gravity, $\phi := \phi_1 + \cdots + \phi_N$ is the cumulative solids concentration, and $\mathbf{T}_{\mathrm{f}}^{\mathrm{E}}$ is the viscous (or extra) stress tensor of the mixture, which all viscous effects have been "swept" into. Since we pass to one space dimension in a moment, the detailed form of $\mathbf{T}_{\mathrm{f}}^{\mathrm{E}}$ is unimportant here.

2.2. The flux density vector

The choice of the flux density functions $f_i(\Phi)$, $i = 1, \ldots, N$, reflects the material behavior of the N-disperse suspension under study. In this paper we consider the Masliyah–Lockett–Bassoon (MLB) model [16,53,54], which amounts to utilizing

$$f_i(\Phi) = f_i^{\mathrm{M}}(\Phi) := \mu V(\phi) \phi_i \left[\delta_i (\bar{\varrho}_i - \bar{\varrho}^{\mathrm{T}} \Phi) - \sum_{k=1}^{N} \delta_k \phi_k (\bar{\varrho}_k - \bar{\varrho}^{\mathrm{T}} \Phi) \right], \quad i = 1, \ldots, N. \tag{2.4}$$

Here, the parameters $\mu, \delta_i, \bar{\varrho}_i$ and $\bar{\varrho}$ are defined by $\mu := -g d_1^2/(18\mu_{\mathrm{f}})$, $\delta_i := d_i^2/d_1^2$ and $\bar{\varrho}_i := \varrho_i - \varrho_{\mathrm{f}}$ for $i = 1, \ldots, N$, and $\bar{\varrho} := (\bar{\varrho}_1, \ldots, \bar{\varrho}_N)^{\mathrm{T}}$. The function $V(\phi)$ is a hindered settling function that can, for example, be chosen as the Richardson–Zaki [66] function

$$V(\phi) = \begin{cases} (1-\phi)^{n-2}, & n \geqslant 2 \quad \text{for } 0 \leqslant \phi \leqslant \phi_{\max}, \\ 0 & \text{otherwise}, \end{cases} \tag{2.5}$$

where $0 < \phi_{\max} \leqslant 1$ is a maximum solids concentration.

2.3. Stability of the MLB model

Alternative choices of the flux vector $\mathbf{f}(\Phi)$ are discussed in [8,9]. The study in [46] provides an experimental comparison of five of these models (each one defined by its flux density vector $\mathbf{f}(\Phi)$), including the MLB model, which turned out to predict the separation of a bidisperse suspension with good accuracy but is even outperformed by the algebraically more complicated Patwardhan and Tien model [64].

Our preference of the MLB model is based on recent analyses [6,16], in which we show that the model has desirable stability properties. We briefly discuss this issue. In one space dimension, only Eq. (2.1) need to be solved, with $q \equiv 0$ in a closed column of height L. This leads to the initial-boundary value problem of a system of conservation laws

$$\partial_t \phi_i + \partial_x f_i(\Phi) = 0, \quad i = 1, \ldots, N, \tag{2.6}$$

$$\Phi(x,0) = \Phi_0(x), \ 0 \leqslant x \leqslant L; \quad \mathbf{f}|_{x=0} = \mathbf{f}|_{x=L} = 0, \quad t > 0. \tag{2.7}$$

It is well known that solutions of (2.6) are discontinuous in general, and that the propagation speed $\sigma(\Phi^+, \Phi^-)$ of a discontinuity in the concentration field ϕ_i separating the states Φ^+ and Φ^- is given by the Rankine–Hugoniot condition $\sigma = (f_i(\Phi^+) - f_i(\Phi^-))/(\phi_i^+ - \phi_i^-), \ i = 1, \ldots, N$.

We recall that the system (2.6) is called *hyperbolic* if the eigenvalues of the Jacobian $\mathscr{J}_{\mathbf{f}}(\Phi) := (\partial f_i/\partial \phi_k)_{1 \leqslant i,k \leqslant N}$ are real, and *strictly hyperbolic* if these are moreover pairwise distinct. For $N = 2$, a system with a pair of complex conjugate eigenvalues is *elliptic*. Some of the flux-density vectors $\mathbf{f}(\Phi)$ proposed in the literature cause the system (2.6) to be nonhyperbolic, or to be of mixed hyperbolic-elliptic type in the case $N = 2$, depending on the size and density parameters, where the type is *mixed* if for given sizes and densities, the system is nonhyperbolic (or elliptic) for $\Phi \in E$, $E \subset \mathscr{D} := \{\Phi \in \mathbb{R}^N : \Phi \geqslant 0, \phi \leqslant 1\}$, and $\mathscr{D} \backslash E$ is nonempty.

The ellipticity criterion is equivalent to Batchelor and Janse van Rensburg's [4] criterion for the occurrence of instabilities like blobs and viscous fingering in bidisperse sedimentation. By a perturbation analysis, we showed [16] that loss of hyperbolicity, that is the occurrence of complex eigenvalues of $\mathscr{J}_{\mathbf{f}}(\Phi)$, provides an instability criterion for polydisperse suspensions of *arbitrary* numbers of species N.

More recently [6], we proved that for equal-density particles ($\bar{\varrho}_1 = \cdots = \bar{\varrho}_N = \varrho_s - \varrho_f$), *arbitrary* N and particle size distributions, the system (2.6) is strictly hyperbolic for all $\Phi \in \mathscr{D}$ with $\phi_1 > 0, \ldots, \phi_N > 0$ and $\phi < 1$ if the flux vector (2.4) is chosen. The proof involves evaluating the characteristic polynomial of the Jacobian $\mathscr{J}_{\mathbf{f}}(\Phi)$. This can be done by means of an explicit formula, which in turn is derived by exploiting elimination possibilities in the corresponding determinants. The hyperbolicity, and thus stability result for equal-density spheres is in agreement with experimental evidence since instability phenomena never have been observed with this type of mixtures, but always involve particles of different specific densities.

2.4. The continuous clarifier-thickener

Consider the clarifier-thickener drawn in Fig. 1, which is supposed to have a constant cross-sectional area S. This unit is analogous to that in [10,12,15], but is now supposed to treat a polydisperse suspension. This (of course, highly idealized) vessel is operated in the following way.

At depth $x = 0$, feed suspension is fed into the equipment at a volume rate $Q_F(t) \geqslant 0$. The feed suspension contains solids of Species 1 to N at the corresponding volume fractions $\phi_1^F(t)$ to $\phi_N^F(t)$ satisfying $\phi_i^F(t) \geqslant 0$, $i = 1, \ldots, N$, and $\phi^F(t) := \phi_1^F(t) + \cdots + \phi_N^F(t) \leqslant \phi_{\max}$. At $x = 0$, the feed flow divides into an upwards-directed and a downwards-directed bulk flow. We assume that the underflow volume rate $Q_R(t) \geqslant 0$ is also prescribed, and that $Q_R(t) \leqslant Q_F(t)$. Consequently, the signed volume

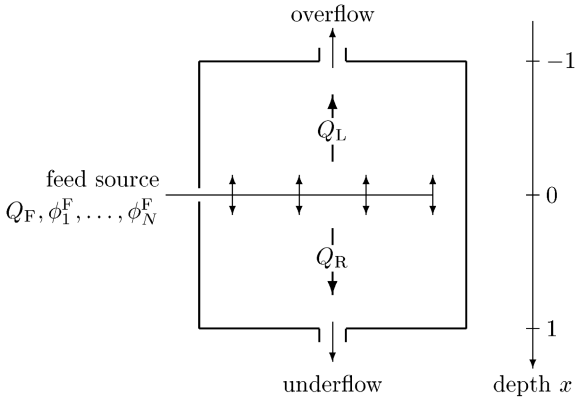

Fig. 1. The clarifier-thickener model showing the known bulk flows and control variables. The upper half ($x \in [-1, 0)$) is the clarification zone and the lower half ($x \in (0, 1]$) is the thickening zone.

rate of the upwards-directed bulk flow is

$$Q_{\mathrm{L}}(t) = Q_{\mathrm{R}}(t) - Q_{\mathrm{F}}(t) \leqslant 0. \tag{2.8}$$

At depth $x = -1$, an overflow opening is located. Summarizing, we prescribe the volume rates $Q_{\mathrm{F}}(t)$ and $Q_{\mathrm{R}}(t)$ and the feed concentrations $\phi_1^{\mathrm{F}}(t)$ to $\phi_N^{\mathrm{F}}(t)$ as independent control variables. From these we calculate the dependent control variable $Q_{\mathrm{L}}(t)$ by (2.8).

For the remainder of the paper, we simply assume that all control variables are constant with respect to t, and we introduce $q_c := Q_c/S$, $c \in \{\mathrm{F}, \mathrm{L}, \mathrm{R}\}$. Moreover, to avoid tedious repetitions, we assume that in all equations the index i assumes the values $i = 1, \ldots, N$, and that $j \in \mathbb{Z}$.

Disregarding for a moment the presence of a solids source but appropriately taking into account these bulk flow velocities, we can write the flux function for Species i as

$$\tilde{g}_i(\Phi, x) = \begin{cases} (q_{\mathrm{R}} - q_{\mathrm{F}})\phi_i & \text{for } x \leqslant -1, \quad q_{\mathrm{R}}\phi_i + f_i^{\mathrm{M}}(\Phi) \quad \text{for } 0 < x \leqslant 1, \\ (q_{\mathrm{R}} - q_{\mathrm{F}})\phi_i + f_i^{\mathrm{M}}(\Phi) & \text{for } -1 < x \leqslant 0, \quad q_{\mathrm{R}}\phi_i \quad \text{for } x > 1. \end{cases} \tag{2.9}$$

Including now the feed mechanism leads to the system of conservation laws with source term $\partial_t \phi_i + \partial_x(\tilde{g}_i(\Phi, x)) = q_{\mathrm{F}}\phi_i^{\mathrm{F}}\delta(x)$, where $\delta(\cdot)$ denotes the Dirac direct mass. Including the singular source term into the flux function and using the Heaviside function $H(\cdot)$ leads to the equation

$$\partial_t \phi_i + \partial_x(\tilde{g}_i(\Phi, x) - q_{\mathrm{F}}\phi_i^{\mathrm{F}} H(x)) = 0. \tag{2.10}$$

We can write (2.10) as $\partial_t \phi_i + \partial_x(\hat{g}_i(\Phi, x)) = 0$ with

$$\hat{g}_i(\Phi, x) := \begin{cases} (q_{\mathrm{R}} - q_{\mathrm{F}})\phi_i & \text{for } x \leqslant -1, \quad q_{\mathrm{R}}\phi_i - q_{\mathrm{F}}\phi_i^{\mathrm{F}} + f_i^{\mathrm{M}}(\Phi) \quad \text{for } 0 < x \leqslant 1, \\ (q_{\mathrm{R}} - q_{\mathrm{F}})\phi_i + f_i^{\mathrm{M}}(\Phi) & \text{for } -1 < x \leqslant 0, \quad q_{\mathrm{R}}\phi_i - q_{\mathrm{F}}\phi_i^{\mathrm{F}} \quad \text{for } x > 1. \end{cases}$$

Adding the constant $-(q_{\mathrm{R}} - q_{\mathrm{F}})\phi_i^{\mathrm{F}}$, we can finally state the initial-value problem of interest as

$$\partial_t \phi_i + \partial_x g_i(\Phi, x) = 0, \quad t > 0, \ x \in \mathbb{R}, \tag{2.11}$$

$$\phi_i(x,0)=\phi_i^0(x),\quad x\in\mathbb{R};\quad \Phi^0\in\mathscr{D}_{\phi_{\max}},\tag{2.12}$$

$$g(\Phi,x)=\begin{cases}(q_{\mathrm{R}}-q_{\mathrm{F}})(\phi_i-\phi_i^{\mathrm{F}}) & \text{for } x\leqslant -1,\\ (q_{\mathrm{R}}-q_{\mathrm{F}})(\phi_i-\phi_i^{\mathrm{F}})+f_i^{\mathrm{M}}(\Phi) & \text{for } -1<x\leqslant 0,\\ q_{\mathrm{R}}(\phi_i-\phi_i^{\mathrm{F}})+f_i^{\mathrm{M}}(\Phi) & \text{for } 0<x\leqslant 1,\\ q_{\mathrm{R}}(\phi_i-\phi_i^{\mathrm{F}}) & \text{for } x>1.\end{cases}\tag{2.13}$$

As in [12,15], the flux discontinuities can be described by two discontinuous parameters

$$\gamma^1(x):=\begin{cases}0 & \text{for } x\notin[-1,1],\\ 1 & \text{for } x\in[-1,1],\end{cases}\qquad \gamma^2(x):=\begin{cases}q_{\mathrm{R}}-q_{\mathrm{F}} & \text{for } x<0,\\ q_{\mathrm{R}} & \text{for } x>0.\end{cases}$$

Collecting the parameters γ^1 and γ^2 in the vector $\gamma(x):=(\gamma^1(x),\gamma^2(x))$, we can write the flux as

$$f_i(\gamma(x),\Phi):=\gamma^1(x)f_i^{\mathrm{M}}(\Phi)+\gamma^2(x)(\phi_i-\phi_i^{\mathrm{F}}),\tag{2.14}$$

such that the governing equation (2.11) takes the form

$$\partial_t\phi_i+\partial_x f_i(\gamma(x),\Phi)=0\quad (i=1,\dots,N).\tag{2.15}$$

2.5. The scalar case

For $N=1$ we identify $\phi=\phi_1=\Phi$, $\bar{\varrho}_1=\bar{\varrho}_{\mathrm{s}}$ and $f^{\mathrm{M}}(\phi)=f_1^{\mathrm{M}}(\phi)$ and obtain from (2.4)

$$f^{\mathrm{M}}(\phi)=\mu V(\phi)\phi(\bar{\varrho}_{\mathrm{s}}(1-\phi)-\phi(\bar{\varrho}_{\mathrm{s}}-\bar{\varrho}_{\mathrm{s}}\phi))=u_\infty\phi(1-\phi)^2V(\phi),\quad u_\infty=\frac{d^2g(\varrho_{\mathrm{s}}-\varrho_{\mathrm{f}})}{18\mu_{\mathrm{f}}},$$

where u_∞ is (according to Stokes' law) the final settling velocity of a sphere of diameter d and density ϱ_{s} in an unbounded fluid of density ϱ_{f} and viscosity μ_{f}. For the function (2.5) we obtain the widely used function $f^{\mathrm{M}}(\phi)=f(\phi)$ given by

$$f(\phi)=\begin{cases}u_\infty\phi(1-\phi)^n & \text{for } 0<\phi<\phi_{\max},\\ 0 & \text{otherwise.}\end{cases}\tag{2.16}$$

The scalar case represents the appropriate extension of Kynch's well-known kinematic theory [45] of one-dimensional batch sedimentation of small rigid spheres to continuous sedimentation. Studies of such models from an applicative point of view and ad-hoc numerical treatments include [3,19,20,47,68], see also [14] for an overview and a brief history of mathematical models of continuous sedimentation. The decisive problem is, of course, the appropriate description and discretization of the singular feed source term and the discontinuous transition between upward and downward directed flows. This problem was circumvented in [19] by smoothing out the source term. On the other hand, Nasr-El-Din et al. [56–58] assume that a feed point source is associated with a "source zone" of finite height within the clarifier-thickener. The obvious purpose of this zone is to act as a "buffer" between the upward and downward directed bulk flows, so that these flows occur in regions which are spatially separated. In fact, it is assumed in [57] (similar statements also appear in [56,58]) that "the solids and the carrier fluid are allowed to exit through the overflow or the underflow boundaries, but they are not allowed to enter the source zone except through the feed

stream". These assumptions are however not put in mathematical terms in [56–58]. Moreover, a model in which the clarification and thickening zones are not connected is clearly unable to explain the really interesting cases, which occur for example if solids accumulate in the thickening zone, form a rising sediment layer, and eventually break through the feed level ($x = 0$). (The mentioned papers [56–58] are concerned with polydisperse suspensions, but the shortcomings of the "source zone" concept are independent of the aspect of polydispersivity.)

Thorough analyzes of the clarifier-thickener model with discontinuous flux (as presented here) for the scalar case ($N = 1$), constructions of solutions, and operating charts predicting the behavior of the system in response to operating conditions were presented by Diehl in a series of papers [21–25]. Complementing the insight provided by these analyses by a computational approach, the authors and co-workers have formulated several alternative numerical methods that can be employed to solve the clarifier-thickener model in the monodisperse (scalar) case. A front tracking scheme is analyzed in [10], a scalar finite difference scheme is analyzed in [12,15], its extension to vessels with discontinuously varying cross-sectional area is treated in [13,14], while a relaxation scheme is analyzed in [11]. A complete existence and uniqueness theory in a particular functional class is given in [15].

3. Central schemes

Roughly speaking, shock-capturing numerical schemes for systems of conservation laws can be classified as either central schemes or upwind schemes. A disadvantage with upwind schemes is that one needs to solve the Riemann problem exactly or approximately, which is difficult for complicated systems. We point out that the (exact or approximate) solution of the Riemann problem for the system of conservation laws that we study in this paper is not known at the moment. For this reason, we turned our attention to central schemes in our previous papers [8,9] on systems of conservation laws (without discontinuous coefficients) modeling sedimentation of polydisperse suspensions. In the 1990s, this central class of schemes received considerable interest, following the introduction of the second-order sequel to the Lax–Friedrichs scheme in [59]. Second-order central schemes can be viewed as a direct extension of the first-order Lax–Friedrichs central scheme, which is known to be robust but contains excessive dissipation. Second-order central schemes resolve the problem of excessive dissipation by reconstructing, in each time step, a (MUSCL type) piecewise-linear interpolant from the cell averages computed in the previous time step. Unlike upwind schemes, central schemes avoid approximate Riemann solvers, projections along characteristic directions, and the splitting of the flux vector in upwind and downwind directions. This makes them attractive for solving involved systems of conservation laws such as the system that we consider in this paper. In [8], we used the second-order shock-capturing scheme developed in [59], while in [9] we used the second-order scheme developed in [44], which we refer to as the KT scheme. In this paper, as in [9], we shall continue to use the KT scheme [44]. The KT scheme has a smaller numerical viscosity and is better suited for near steady-state calculations that the original central scheme [59], a property that is relevant for our application. Of course, the new feature here is that we adapt the KT scheme to systems with discontinuous flux. We refer to the lecture notes [69] for a general introduction to central schemes and relevant references.

3.1. Derivation of the fully discrete scheme

We introduce a discretization of $\mathbb{R}\times\mathbb{R}^+$ by setting $x_j := j\Delta x$, $j\in\mathbb{Z}$, and $t_n := n\Delta t$, $n\in\mathbb{N}$, $\Delta x,\Delta t>0$, $\lambda := \Delta t/\Delta x$. To derive a numerical scheme for (2.15), we consider the extended system (see Section 1 for motivation)

$$\partial_t\gamma(x)=\partial_t(\gamma^1(x),\gamma^2(x))^{\mathrm{T}}=0,$$

$$\partial_t\phi_i+\partial_x f_i(\gamma(x),\Phi)=0\quad(i=1,\dots,N).$$

We introduce the vector of unknowns $\mathbf{u}\in\mathbb{R}^{N+2}$ by $\mathbf{u} := (\phi_1,\dots,\phi_N,u_{N+1},u_{N+2})^{\mathrm{T}}$ and the corresponding flux vector $\mathbf{F}:\mathbb{R}^{N+2}\to\mathbb{R}^{N+2}$ by

$$\mathbf{F}(\mathbf{u}) := (f_1(\phi_1,\dots,\phi_N,u_{N+1},u_{N+2}),\dots,f_N(\phi_1,\dots,\phi_N,u_{N+1},u_{N+2}),0,0)^{\mathrm{T}},\tag{3.1}$$

where the functions f_1 to f_N are defined by (2.14), with γ^1 and γ^2 replaced by u_{N+1} and u_{N+2}, respectively. Note that $\mathbf{F}$ does not depend on x. We then consider the initial value problem

$$\partial_t\mathbf{u}+\partial_x\mathbf{F}(\mathbf{u})=0,\quad x\in\mathbb{R},\ t>0,\tag{3.2}$$

$$\mathbf{u}(x,0)=\mathbf{u}_0(x),\quad x\in\mathbb{R};\quad \mathbf{u}_0(x)=(\phi_1^0(x),\dots,\phi_N^0(x),\gamma^1(x),\gamma^2(x))^{\mathrm{T}}.\tag{3.3}$$

We now construct a numerical scheme by applying the KT scheme [44] to the initial-value problem (3.2), (3.3). To this end, assume that at time level t_n we are given the cell averages $\{\bar{\mathbf{u}}_j^n\}=\{(\bar\phi_{1,j}^n,\dots,\bar\phi_{N,j}^n,\bar u_{N+1,j}^n,\bar u_{N+2,j}^n)^{\mathrm{T}}\}$. We then construct a piecewise linear reconstruction

$$\mathbf{u}(x,t_n)=\sum_{j\in\mathbb{Z}}\left(\bar{\mathbf{u}}_j^n+\frac{1}{\Delta x}\mathbf{u}_j'(x-x_j)\right)\chi_{[x_{j-1/2},x_{j+1/2}]}(x),\tag{3.4}$$

where the slope vector $\mathbf{u}_j'=(\phi_{1,j}',\dots,\phi_{N,j}',u_{N+1,j}',u_{N+2,j}')^{\mathrm{T}}$ is defined by

$$\phi_{l,j}'=\mathrm{MM}\{\theta(\bar\phi_{l,j}^n-\bar\phi_{l,j-1}^n),(\bar\phi_{l,j+1}^n-\bar\phi_{l,j-1}^n)/2,\theta(\bar\phi_{l,j+1}^n-\bar\phi_{l,j}^n)\},\quad l=1,\dots,N,\tag{3.5}$$

$$u_{l,j}'=\mathrm{MM}\{\theta(\bar u_{l,j}^n-\bar u_{l,j-1}^n),(\bar u_{l,j+1}^n-\bar u_{l,j-1}^n)/2,\theta(\bar u_{l,j+1}^n-\bar u_{l,j}^n)\},\quad l=N+1,N+2,\tag{3.6}$$

where $\theta\in[0,2]$ is a parameter and $\mathrm{MM}(\cdot,\cdot,\cdot)$ denotes the usual minmod function which equals $\min\{a,b,c\}$ if $a,b,c>0$, $\max\{a,b,c\}$ if $a,b,c<0$, and zero otherwise. In particular, this choice of slope vectors satisfies (see [59]) $(1/\Delta x)\mathbf{u}_j'=(\partial\mathbf{u}/\partial x)(x=x_j,t=t_n)+\mathcal{O}(\Delta x)$, which ensures second-order accuracy wherever the components of $\mathbf{u}$ are smooth.

The new ingredient of the KT scheme [44] is an estimate of the local propagation speeds $a_{j+1/2}^n$, $j\in\mathbb{Z}$ at the cell boundaries $x_{j+1/2}$, $j\in\mathbb{Z}$. We define the left and right intermediate values of the interpolant $\mathbf{u}(x,t_n)$ at $x=x_{j+1/2}$ by

$$\bar{\mathbf{u}}_{j+1/2}^- := \mathbf{u}(x_{j+1/2}^-,t_n)=\bar{\mathbf{u}}_j^n+\frac{1}{2}\mathbf{u}_j',\quad \bar{\mathbf{u}}_{j+1/2}^+ := \mathbf{u}(x_{j+1/2}^+,t_n)=\bar{\mathbf{u}}_{j+1}^n-\frac{1}{2}\mathbf{u}_{j+1}'.$$

We denote by $\rho(\cdot)$ the spectral radius function and by $\mathcal{J}_{\mathbf{F}}(\mathbf{u})$ the $(N+2)\times(N+2)$ Jacobian of $\mathbf{F}(\mathbf{u})$. Then according to [44] the local speeds of propagation are defined by

$$a_{j+1/2}^n=\max\{\rho(\mathcal{J}_{\mathbf{F}}(\mathbf{u}_{j+1/2}^-)),\rho(\mathcal{J}_{\mathbf{F}}(\mathbf{u}_{j+1/2}^+))\}.\tag{3.7}$$

In practice, the quantities $a^n_{j+1/2}$ are estimated by considering 'approximate eigenvalues'. However, in the particular case of the MLB model with equal-density spheres and for arbitrary N, accurate bounds for these eigenvalues are available, see [6].

Given the piecewise linear interpolant $\mathbf{u}(\cdot,t_n)$ defined in (3.4) and the local speeds $a_{j+1/2}$, the construction of the cell averages $\bar{\mathbf{u}}^{n+1}_j$ proceeds in two steps as follows.

Step 1: The original central scheme due to Nessyahu and Tadmor [59] is based on averaging over the (staggered) control volume $[x_j, x_{j+1}]$ of fixed size Δx. Instead, we here integrate over the narrower (and nonuniform) control volume $[x^n_{j+1/2,\mathrm{l}}, x^n_{j+1/2,\mathrm{r}}] \subset [x_j, x_{j+1}]$, where $x^n_{j+1/2,\mathrm{l}} := x_{j+1/2} - a^n_{j+1/2}\Delta t$ and $x^n_{j+1/2,\mathrm{r}} := x_{j+1/2} + a^n_{j+1/2}\Delta t$. We now introduce two families of cell averages at time level t_{n+1}, namely the averages

$$\bar{\boldsymbol{\Psi}}^{n+1}_{j+1/2} := \frac{1}{\Delta x^n_{j+1/2}} \int_{x^n_{j+1/2,\mathrm{l}}}^{x^n_{j+1/2,\mathrm{r}}} \mathbf{u}(x, t_{n+1})\,\mathrm{d}x, \tag{3.8}$$

which contain the information from the Riemann fans emerging from the cell boundaries x_j at time t_n, and the averages

$$\bar{\boldsymbol{\Psi}}^{n+1}_{j} := \frac{1}{\Delta x^n_{j}} \int_{x^n_{j-1/2,\mathrm{r}}}^{x^n_{j+1/2,\mathrm{l}}} \mathbf{u}(x, t_{n+1})\,\mathrm{d}x,$$

$$\Delta x^n_j := x^n_{j+1/2,\mathrm{l}} - x^n_{j-1/2,\mathrm{r}} = \Delta x - \Delta t(a^n_{j-1/2} + a^n_{j+1/2}), \tag{3.9}$$

that are free of neighboring Riemann fans. Inserting the definition (3.4) of the piecewise linear reconstruction, we obtain for the first family of cell averages the equation

$$\begin{aligned}\bar{\boldsymbol{\Psi}}^{n+1}_{j+1/2} = {} & \frac{1}{2}(\bar{\mathbf{u}}^n_j + \bar{\mathbf{u}}^n_{j+1}) + \frac{1}{4}(1 - a^n_{j+1/2}\lambda)(\mathbf{u}'_j - \mathbf{u}'_{j+1}) \\ & - \frac{1}{2a^n_{j+1/2}\Delta t}\left[\int_{t_n}^{t_{n+1}} \mathbf{F}(\mathbf{u}(x^n_{j+1/2,\mathrm{r}}))\,\mathrm{d}t - \int_{t_n}^{t_{n+1}} \mathbf{F}(\mathbf{u}(x^n_{j+1/2,\mathrm{l}}))\,\mathrm{d}t\right].\end{aligned} \tag{3.10}$$

Applying the midpoint rule to approximate the time integrals in (3.10), we get

$$\bar{\boldsymbol{\Psi}}^{n+1}_{j+1/2} = \frac{1}{2}(\bar{\mathbf{u}}^n_j + \bar{\mathbf{u}}^n_{j+1}) + \frac{1 - a^n_{j+1/2}\lambda}{4}(\mathbf{u}'_j - \mathbf{u}'_{j+1}) - \frac{1}{2a^n_{j+1/2}}(\mathbf{F}(\mathbf{u}^{n+1/2}_{j+1/2,\mathrm{r}}) - \mathbf{F}(\mathbf{u}^{n+1/2}_{j+1/2,\mathrm{l}})), \tag{3.11}$$

where the mid-point values are obtained by Taylor expansions:

$$\begin{aligned}&\mathbf{u}^{n+1/2}_{j+1/2,\mathrm{l}} := \mathbf{u}^n_{j+1/2,\mathrm{l}} - \frac{\lambda}{2}\mathbf{F}'(\mathbf{u}^n_{j+1/2,\mathrm{l}}), \quad \mathbf{u}^{n+1/2}_{j+1/2,\mathrm{r}} := \mathbf{u}^n_{j+1/2,\mathrm{r}} - \frac{\lambda}{2}\mathbf{F}'(\mathbf{u}^n_{j+1/2,\mathrm{r}}), \\ &\mathbf{u}^n_{j+1/2,\mathrm{l}} := \bar{\mathbf{u}}^n_j + \left(\frac{1}{2} - \lambda a^n_{j+1/2}\right)\mathbf{u}'_j, \quad \mathbf{u}^n_{j+1/2,\mathrm{r}} := \bar{\mathbf{u}}^n_{j+1} - \left(\frac{1}{2} - \lambda a^n_{j+1/2}\right)\mathbf{u}'_{j+1},\end{aligned} \tag{3.12}$$

and the components of the slope vectors (introduced with a slight abuse of notation)

$$\mathbf{F}'(\mathbf{u}^n_{j+1/2,c}) = (F'_1(\mathbf{u}^n_{j+1/2,c}), F'_2(\mathbf{u}^n_{j+1/2,c}), \ldots, F'_{N+2}(\mathbf{u}^n_{j+1/2,c}))^{\mathrm{T}}, \quad c \in \{\mathrm{l},\mathrm{r}\}$$

are calculated by

$$\begin{aligned}F'_l(\mathbf{u}^n_{j+1/2,c}) = \mathrm{MM}\{&\theta(F_l(\mathbf{u}^n_{j+1/2,c}) - F_l(\mathbf{u}^n_{j-1/2,c})), (F_l(\mathbf{u}^n_{j+3/2,c}) - F_l(\mathbf{u}^n_{j-1/2,c}))/2, \\ &\theta(F_l(\mathbf{u}^n_{j+3/2,c}) - F_l(\mathbf{u}^n_{j+1/2,c}))\}, \quad c \in \{\mathrm{l},\mathrm{r}\},\ l = 1,\ldots,N+2.\end{aligned} \tag{3.13}$$

The second family of cell averages defined by (3.9) is handled in a similar way. As before, integrating exactly and then approximating the resulting two time integrals by the midpoint rule, we get the following equation for the cell averages (3.9):

$$\bar{\Psi}_j^{n+1} = \bar{\mathbf{u}}_j^n - \frac{\lambda}{4}(a_{j+1/2}^n - a_{j-1/2}^n)\mathbf{u}_j' - \frac{\lambda}{1-\lambda(a_{j-1/2}^n + a_{j+1/2}^n)}(\mathbf{F}(\mathbf{u}_{j+1/2,\mathrm{l}}^{n+1/2}) - \mathbf{F}(\mathbf{u}_{j-1/2,\mathrm{r}}^{n+1/2})), \tag{3.14}$$

where the vectors $\mathbf{u}_{j+1/2,\mathrm{l}}^{n+1/2}$ and $\mathbf{u}_{j-1/2,\mathrm{r}}^{n+1/2}$ are defined in (3.12).

Step 2: In the second (and final) step, we convert the nonuniform cell averages (3.8) and (3.9) into cell averages over the nonstaggered grid cells $[x_{j-1/2}, x_{j+1/2}]$, $j \in \mathbb{Z}$. To this end, we consider a piecewise linear reconstruction over the nonuniform grid cells at time t_{n+1} and then project its averages onto the original grid. The required piecewise linear reconstruction takes the form

$$\begin{aligned}\Psi(x, t_{n+1}) = &\sum_{j\in\mathbb{Z}} (\bar{\Psi}_{j+1/2}^{n+1} + \Psi'_{j+1/2}(x - x_{j+1/2}))\chi_{[x_{j+1/2,\mathrm{l}}^n, x_{j+1/2,\mathrm{r}}^n]}(x) \\ &+ \sum_{j\in\mathbb{Z}} \bar{\Psi}_j^{n+1}\chi_{[x_{j-1/2,\mathrm{r}}^n, x_{j+1/2,\mathrm{l}}^n]}(x),\end{aligned} \tag{3.15}$$

where the discrete derivative vector $\Psi'_{j-1/2} = (\psi'_{1,j+1/2}, \ldots, \psi'_{N+2,j+1/2})^{\mathrm{T}}$ is defined by

$$\begin{aligned}\psi'_{l,j+1/2} = \frac{2}{\Delta x}\mathrm{MM}\Bigg\{ &\frac{\theta(\bar{\psi}_{l,j+1/2}^{n+1} - \bar{\psi}_{l,j}^{n+1})}{1+\lambda(a_{j+1/2}^n - a_{j-1/2}^n)}, \frac{\bar{\psi}_{l,j+1}^{n+1} - \bar{\psi}_{l,j}^{n+1}}{2+\lambda(2a_{j+1/2}^n - a_{j-1/2}^n - a_{j+3/2}^n)}, \\ &\frac{\theta(\bar{\psi}_{l,j+1}^{n+1} - \bar{\psi}_{l,j+1/2}^{n+1})}{1+\lambda(a_{j+1/2}^n - a_{j+3/2}^n)}\Bigg\}, \quad \theta \in [0,2],\ l = 1, \ldots, N+2.\end{aligned} \tag{3.16}$$

One should keep in mind that $\bar{\Psi}_j^{n+1}$ and $\bar{\Psi}_{j+1/2}^{n+1}$ are averages over grid cells centered around

$$x = \frac{1}{2}(x_{j-1/2,\mathrm{r}}^n + x_{j-1/2,\mathrm{l}}^n) = \frac{1}{2}(x_{j-1/2} + x_{j+1/2}) + \frac{\Delta t}{2}(a_{j-1/2}^n - a_{j+1/2}^n)$$

and $x = x_{j+1/2}$, respectively.

Note that simple averaging over $[x_{j-1/2}, x_{j+1/2}]$ reduces the accuracy of the (resulting) scheme to first order. Thus, we need to use the piecewise linear reconstruction (3.15) in order not to loose second-order accuracy when converting the nonuniform cell averages (3.8) and (3.9) into cell averages over the nonstaggered cells $[x_{j-1/2}, x_{j+1/2}]$. Moreover, note that it is not necessary to reconstruct on the intervals $[x_{j-1/2,\mathrm{r}}^n, x_{j+1/2,\mathrm{l}}^n]$ since the solution is smooth there.

Finally, the new cell averages

$$\bar{\mathbf{u}}_j^{n+1} = \frac{1}{\Delta x}\int_{x_{j-1/2}}^{x_{j+1/2}} \Psi(x, t_{n+1})\,\mathrm{d}x$$

are obtained by averaging (3.15), which leads to

$$\begin{aligned}\bar{\mathbf{u}}_j^{n+1} = &\lambda(a_{j-1/2}^n \bar{\Psi}_{j-1/2}^{n+1} + a_{j+1/2}^n \bar{\Psi}_{j+1/2}^{n+1}) + [1 - \lambda(a_{j-1/2}^n + a_{j+1/2}^n)]\bar{\Psi}_j^{n+1} \\ &+ \frac{\Delta x}{2}((\lambda a_{j-1/2}^n)^2 \Psi'_{j-1/2} - (\lambda a_{j+1/2}^n)^2 \Psi'_{j+1/2}).\end{aligned} \tag{3.17}$$

So far the exposition of the scheme has followed the derivation in [9]. We are now interested in identifying the resulting "marching formula" for the last two components u_{N+1} and u_{N+2} of the vector of unknowns $\mathbf{u}$, for which the corresponding components F_{N+1} and F_{N+2} of the flux vector $\mathbf{F}(\mathbf{u})$ are zero. To this end, first observe that for these components the equations for the cell averages (3.11) and (3.14) become

$$\bar{\psi}^{n+1}_{l,j+1/2} = \frac{1}{2}(\bar{u}^n_{l,j} + \bar{u}^n_{l,j+1}) + \frac{1}{4}(1 - a^n_{j+1/2}\lambda)(u'_{l,j} - u'_{l,j+1}),$$

$$\bar{\psi}^{n+1}_{l,j} = \bar{u}^n_{l,j} - \frac{\lambda}{2}(a^n_{j+1/2} - a^n_{j-1/2})u'_{l,j} \quad \text{for } l = N+1, N+2. \tag{3.18}$$

From (3.17) we obtain for $l = N+1, N+2$

$$\bar{u}^{n+1}_{l,j} = \lambda(a^n_{j-1/2}\bar{\psi}^{n+1}_{l,j-1/2} + a^n_{j+1/2}\bar{\psi}^{n+1}_{l,j+1/2}) + (1 - \lambda(a^n_{j-1/2} + a^n_{j+1/2}))\bar{\psi}^{n+1}_{l,j}$$
$$+ \frac{\Delta x}{2}((\lambda a^n_{j-1/2})^2\psi'_{l,j-1/2} - (\lambda a^n_{j+1/2})^2\psi'_{l,j+1/2}). \tag{3.19}$$

Inserting (3.18) we obtain the scheme for the evolution of the variables u_{N+1} and u_{N+2} representing the discontinuity parameters γ^1 and γ^2:

$$\bar{u}^{n+1}_{l,j} = \left(1 - \frac{\lambda}{2}(a^n_{j-1/2} + a^n_{j+1/2})\right)\bar{u}^n_{l,j} + \frac{\lambda}{2}a^n_{j-1/2}\bar{u}^n_{l,j-1} + \frac{\lambda}{2}a^n_{j+1/2}\bar{u}^n_{l,j+1}$$
$$+ \frac{\lambda}{4}[(a^n_{j+1/2} - a^n_{j-1/2})(\lambda(a^n_{j+1/2} + a^n_{j-1/2}) - 1)u'_{l,j} + a^n_{j-1/2}(1 - \lambda a^n_{j-1/2})u'_{l,j-1}$$
$$- a^n_{j+1/2}(1 - \lambda a^n_{j+1/2})u'_{l,j+1}] + \frac{\lambda^2\Delta x}{2}((a^n_{j-1/2})^2\psi'_{l,j-1/2} - (a^n_{j+1/2})^2\psi'_{l,j+1/2})$$

for $l = N+1, N+2$. The scheme for ϕ_1 to ϕ_N follows by simply taking the components 1 to N of (3.17). It is instructive to rewrite the marching formula for $\mathbf{u} = (\phi_1, \ldots, \phi_N, u_{N+1}, u_{N+2})^{\mathrm{T}}$ in conservative form. For the combined vector $\mathbf{u}$, the scheme can be written as

$$\bar{\mathbf{u}}^{n+1}_j = \bar{\mathbf{u}}^n_j - \lambda(\mathscr{F}^n_{j+1/2} - \mathscr{F}^n_{j-1/2}), \tag{3.20}$$

where the components of the numerical flux vectors $\mathscr{F} = (\mathscr{F}_1, \mathscr{F}_2, \mathscr{F}_3, \ldots, \mathscr{F}_{N+2})^{\mathrm{T}}$ are given by

$$\mathscr{F}_{l,j+1/2}$$
$$= \frac{1}{2}(f_l(\phi^{n+1/2}_{1,j+1/2,\mathrm{r}}, \ldots, \phi^{n+1/2}_{N,j+1/2,\mathrm{r}}, u^{n+1/2}_{N+1,j+1/2,\mathrm{r}}, u^{n+1/2}_{N+2,j+1/2,\mathrm{r}})$$
$$+ f_l(\phi^{n+1/2}_{1,j+1/2,\mathrm{l}}, \ldots, \phi^{n+1/2}_{N,j+1/2,\mathrm{l}}, u^{n+1/2}_{N+1,j+1/2,\mathrm{l}}, u^{n+1/2}_{N+2,j+1/2,\mathrm{l}}))$$
$$- \frac{a^n_{j+1/2}}{2}(\bar{u}^n_{l,j+1} - \bar{u}^n_{l,j}) + \frac{a^n_{j+1/2}}{4}(1 - \lambda a^n_{j+1/2})(u'_{l,j} + u'_{l,j+1})$$
$$+ \frac{\lambda\Delta x}{2}(a^n_{j+1/2})^2\psi'_{l,j+1/2} \quad \text{for } l = 1, \ldots, N, \tag{3.21}$$

$$\mathscr{F}^n_{l,j+1/2} = -\frac{a^n_{j+1/2}}{2}(\bar{u}^n_{l,j+1} - \bar{u}_{l,j}) + \frac{a^n_{j+1/2}}{4}(1 - \lambda a^n_{l,j+1/2})(u'_{l,j} + u'_{l,j+1}) + \frac{\lambda\Delta x}{2}(a^n_{j+1/2})^2\psi'_{l,j+1/2} \quad \text{for } l = N+1, N+2. \tag{3.22}$$

The extension of the CFL stability condition for the explicit KT scheme stated in [44] for scalar equations to the present system is

$$\frac{\Delta t}{\Delta x}\max\rho(\mathscr{J}_{\mathbf{f}}(\Phi)) \leqslant \frac{1}{8}. \tag{3.23}$$

It is emphasized that we view (3.23) as a necessary condition for the present explicit KT scheme to produce a physically relevant numerical result, and that no rigorous convergence result is associated with (3.23).

3.2. Semi-discrete formulation

The scheme defined by (3.20)–(3.22) is just the KT scheme [44] applied to the particular system (3.1)–(3.3). Thus, as the original scheme, it also admits a semi-discrete version. To derive it, we rewrite (3.20) as

$$\frac{1}{\Delta t}(\bar{\mathbf{u}}^{n+1}_j - \bar{\mathbf{u}}^n_j) = -\frac{1}{\Delta x}(\mathscr{F}^n_{j+1/2} - \mathscr{F}^n_{j-1/2}), \tag{3.24}$$

insert the expressions (3.22) and (3.21) into the right-hand side, and consider the limit $\Delta t \to 0$, for which all $\mathscr{O}(\lambda)$ terms on the right-hand side disappear. To compactly formulate the result of this procedure, which is performed in a more detailed way in [44], we define

$$\mathbf{u}^+_{j+1/2}(t) := \bar{\mathbf{u}}_{j+1}(t) - \frac{1}{2}\mathbf{u}'_{j+1}(t), \quad \mathbf{u}^-_{j+1/2}(t) := \bar{\mathbf{u}}_j(t) + \frac{1}{2}\mathbf{u}'_j(t). \tag{3.25}$$

Then the semi-discrete central scheme is defined by

$$\frac{\mathrm{d}\bar{u}_{l,j}(t)}{\mathrm{d}t} = \frac{1}{2\Delta x}\{-f_l(\bar{\mathbf{u}}^+_{j+1/2}(t)) - f_l(\bar{\mathbf{u}}^-_{j+1/2}(t)) + f_l(\bar{\mathbf{u}}^+_{j-1/2}(t)) + f_l(\bar{\mathbf{u}}^-_{j-1/2}(t)) + a_{j+1/2}(t)(\bar{u}^+_{l,j+1/2}(t) - \bar{u}^-_{l,j+1/2}(t)) - a_{j-1/2}(t)(\bar{u}^+_{l,j-1/2}(t) - \bar{u}^-_{l,j-1/2}(t))\} \tag{3.26}$$

for $t > 0$ and $l = 1, \ldots, N$ and

$$\frac{\mathrm{d}\bar{u}_{l,j}(t)}{\mathrm{d}t} = \frac{a_{j+1/2}(t)}{2\Delta x}(\bar{u}^+_{l,j+1/2}(t) - \bar{u}^-_{l,j+1/2}(t)) - \frac{a_{j-1/2}(t)}{2\Delta x}(\bar{u}^+_{l,j-1/2}(t) - \bar{u}^-_{l,j-1/2}(t)) \tag{3.27}$$

for $t > 0$ and $l = N+1, N+2$.

3.3. Variants and sub-cases

We shall consider some other variants of the scheme (3.20)–(3.22) as well. An obvious simplification occurs if we assume that the discontinuity parameters are not calculated for each time step but are taken as constants (with respect to time), i.e., we solve the additional conservation laws for

the discontinuous coefficients exactly. Then we only need to consider equations (3.20), (3.21) for the fully discrete scheme or equation (3.26) for its semi-discrete version, where every occurrence of u_{N+1} and u_{N+2} is replaced by suitable (exact) evaluations of the parameters γ^1 and γ^2.

A different simplification is produced by turning off the minmod limiter (for example by choosing $\theta = 0$), and by setting $a^n_{j\pm1/2} = 1/\lambda$. This results in the first-order Lax–Friedrichs scheme,

$$\mathscr{F}_{l,j+1/2} = \frac{1}{2}[f_l(\bar{\mathbf{u}}^n_{j+1}) + f_l(\bar{\mathbf{u}}^n_j)] - \frac{1}{2\lambda}(\bar{u}^n_{l,j+1} - \bar{u}^n_{l,j}) \quad \text{for } l = 1,\dots,N, \tag{3.28}$$

$$\mathscr{F}_{l,j+1/2} = -\frac{1}{2\lambda}(\bar{u}^n_{l,j+1} - \bar{u}^n_{l,j}) \quad \text{for } l = N+1, N+2. \tag{3.29}$$

Finally, also here we may disregard the approximate evolution of u_{N+1} and u_{N+2} and simply replace these variables by exact evaluations of the parameters $\gamma^1(x)$ and $\gamma^2(x)$, so that only the scheme defined by (3.20) and (3.28) needs to be used.

4. Numerical examples

4.1. The scalar case and error study

For the error study we select one of the scalar examples that were already considered for illustration of front tracking, upwind difference and relaxation schemes in [10,11]. We consider the flux density function (2.16) with $u_\infty = 6.75$, $\phi_{\max} = 1$ and $n = 2$ and the control parameters $q_{\mathrm{L}} = -1$, $q_{\mathrm{R}} = 0.6$ and $\phi^{\mathrm{F}} = 0.8$, corresponding to a hypothetical material and chosen here merely to make comparison with previous results possible. The vessel is considered to be initially full of water, $\phi_0 = 0$.

We here consider six different schemes: the fully discrete first-order in time KT scheme (3.20), (3.21) with exact evolution of the discontinuity parameters (KT1A), the same scheme except that we employ approximate evolution of the discontinuity parameters via formula (3.22) (KT1B), the semi-discrete KT scheme combined with a second-order Runge–Kutta time discretization with exact evolution of discontinuity parameters (such that only formula (3.26) is used) (KT2A), the same scheme including approximate evolution of the discontinuity parameters via formula (3.27) (KT2B), the first-order Lax–Friedrichs scheme (3.20), (3.28) with the exact evolution of the discontinuity parameters (LxFA), and finally the same scheme with approximate evolution discontinuity parameters by formula (3.29) (LxFB). In all calculations we use $\lambda = 0.015$ and $\theta = 1.3$ for the KT schemes, and denote by J the number of cells into which the "interior" interval $[-1, 1]$ is divided into, i.e. $\Delta x = 2/J$.

The scheme KT2B was selected to compute the reference solution of the problem to be used for the error study. The discretization of the reference solution is given by $J = 4800$. Fig. 2 shows a three-dimensional plot of this solution, where the visual grid used for display is of course much coarser than the computational, and the same solution represented by iso-concentration lines. The merger of such lines indicates a shock. Physically, the solution shows how the thickening zone ($0 \leqslant x \leqslant 1$) is filled up, and that at the same time a solids flux into the clarification zone ($-1 \leqslant x \leqslant 0$) is produced. The solids in part leave the unit through the discharge opening and in part form a rising sediment, which forms a curved shock. At about $t = 1.2$, this shock breaks through the feed level, after some further interaction travels upward at constant speed, and reaches

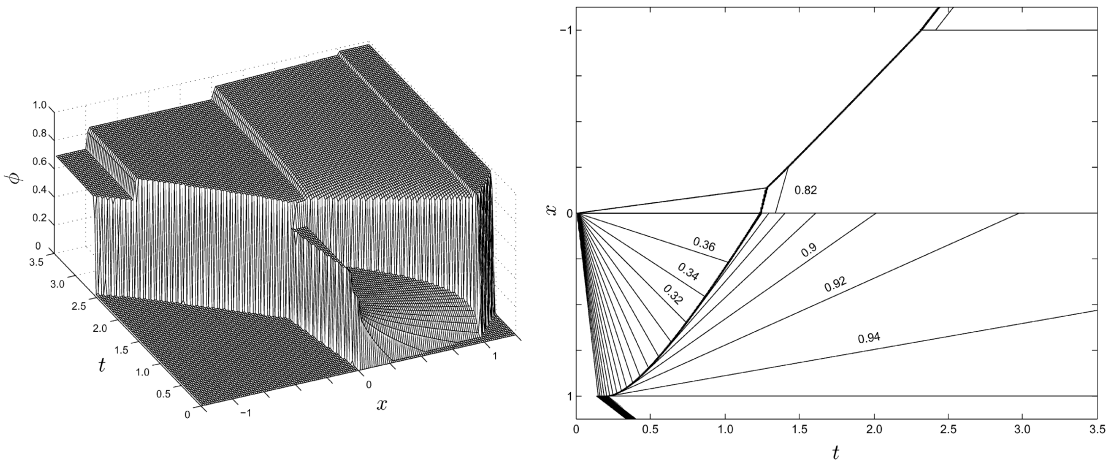

Fig. 2. Example 1: Reference solution ($J = 4800$) used for the error analysis, showing the fill-up and overflow of an ideal clarifier-thickener. The iso-concentration lines correspond to $\phi = 0, 0.02, 0.04, \ldots, 0.96, 0.98, 1$.

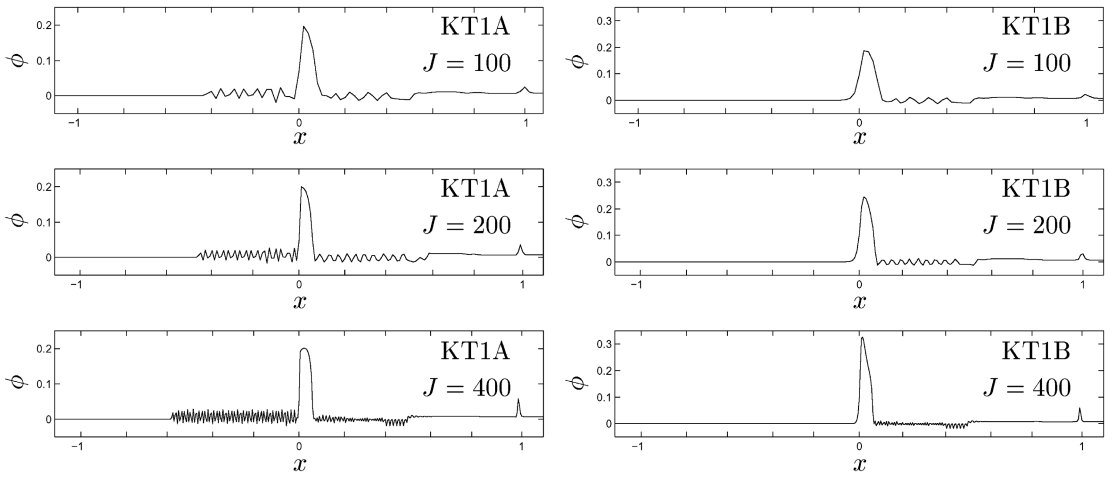

Fig. 3. Example 1: Oscillatory solutions of $u(x, 0.0006)$ produced by the first-order schemes KT1A and KT1B with $\lambda = 0.015$.

the overflow level at about $t = 2.3$. This case has also been used to illustrate several alternative schemes, see [10,11]. The numerical result is consistent with solutions constructed in [24].

As combinations of a second-order spatial with a first-order in time discretizations, the fully discrete KT1A and KT1B schemes produce spurious oscillations. These oscillations were almost invisible in the examples of polydisperse batch sedimentation (not involving discontinuous fluxes) presented in [9]. Fig. 3 illustrates that for the present example, however, these schemes almost instantaneously produce solutions with spurious oscillations, which are apparently caused by the flux discontinuity sitting at $x = 0$. It would possibly be interesting to study the cause of these oscillation, but since we have better schemes available (to be discussed in the sequel), we simply exclude the

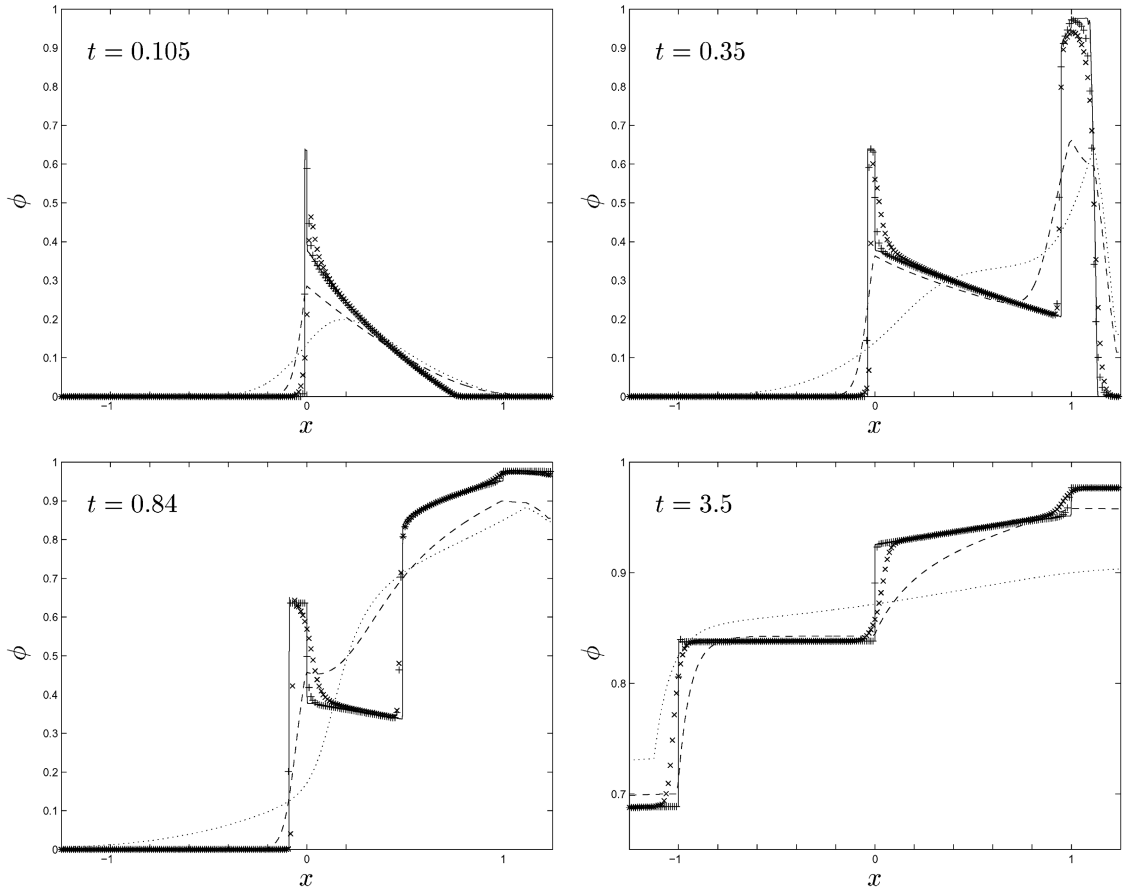

Fig. 4. Example 1: Numerical solution at four different times calculated by LxFA (dashed), LxFB (dotted), KT2A (+) and KT2B (×) with $J = 200$. The solid line represents the reference solution.

KT1A and KT1B schemes from the detailed error study. Observe, however, that KT1A leads to oscillations on both sides of $x = 0$ (where the jump in γ^2 sits), while KT1B leads to oscillations only for $x > 0$ and the solution value zero on the other side of the peak around $x = 0$ is correctly reproduced.

Fig. 4 displays the solution of the schemes KT2A, KT2B, LxFA and LxFB, taken at four different times and calculated with $J = 200$. The 'exact' reference solution is shown as well. Clearly, the (discontinuous) profiles of the 'exact' solution are approximated much better by the second order KT schemes than by the LxF schemes, since the latter are affected by strong numerical diffusion and are smeared out. This effect is, however, in part related to the very low mesh size ratio $\lambda = 0.015$, which was chosen to be consistent with the CFL condition for the KT schemes indicated in [44]. For our example, the schemes produced reasonable approximations, with those of the LxF schemes being less smeared out, also for much higher values of λ.

Fig. 5 shows the global solution calculated by these schemes with $J = 400$. Again observe that the solution produced by the second-order schemes is significantly more accurate than those of the

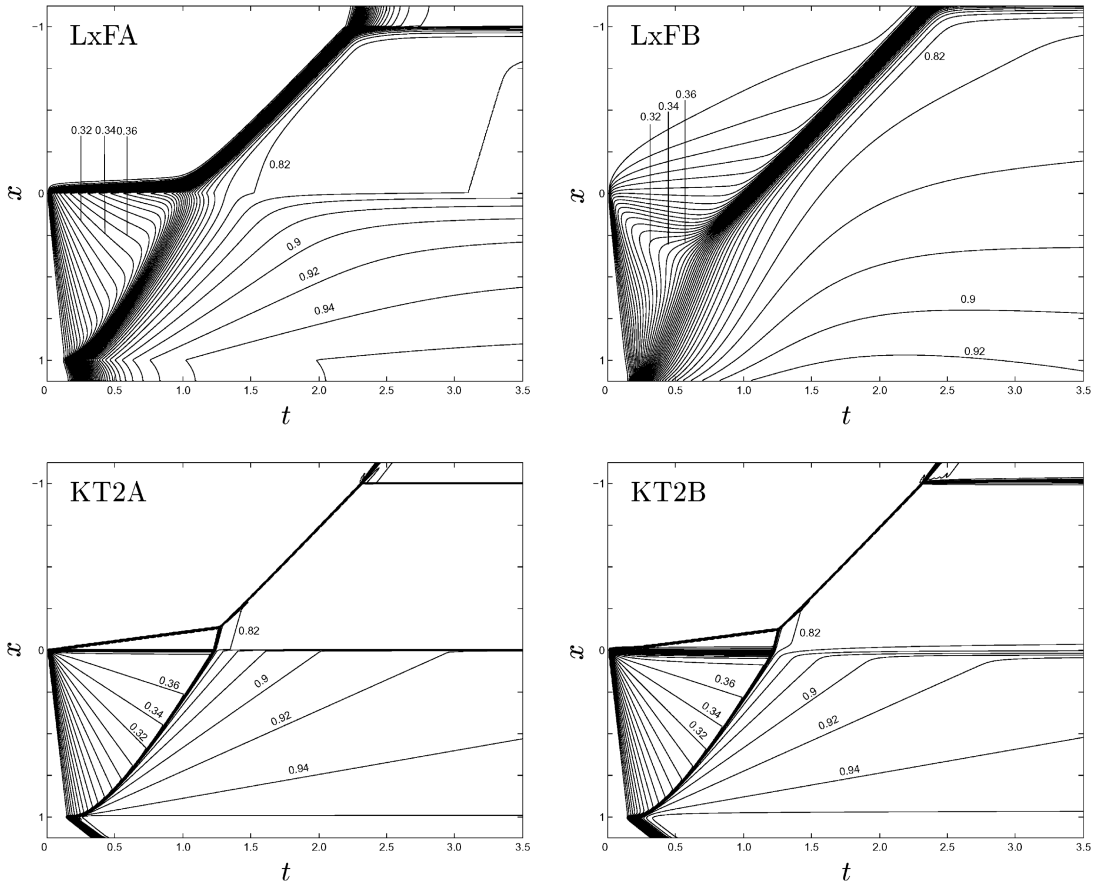

Fig. 5. Example 1: Iso-concentration lines produced by the indicated schemes with $J = 400$ and $\lambda = 0.015$. The lines correspond to the solution values $\phi = 0, 0.02, 0.04, \ldots, 0.98, 1.0$.

first-order schemes, and that keeping the evolution of the discontinuity parameters exact (in the KT2A and LxFA schemes) also leads to more accurate solutions.

We now turn to a quantitative study of the error produced by these four schemes. If ϕ^{Δ} denotes the approximate solution referring to the discretization parameters $\Delta = (\Delta x, \Delta t)$ for a given scheme and ϕ is the exact solution, then the correct error expression should be

$$\tilde{e}(t) = \int_{\mathbb{R}} |\phi^{\Delta}(x,t) - \phi(x,t)| \, \mathrm{d}x.$$

In lack of an exact solution, we replace ϕ by the reference solution ϕ_{ref} calculated with $J = 4800$ and calculate the L^1 error given by

$$e(t) = \int_{-1.045}^{1.045} |\phi^{\Delta}(x,t) - \phi_{\mathrm{ref}}(x,t)| \, \mathrm{d}x.$$

Table 1
Example 1: L^1 errors $e(t)$ and calculated convergence rates (cr) for the times used in Fig. 4

t	J	LxFA $e(t)$	cr	LxFB $e(t)$	cr	KT2A $e(t)$	cr	KT2B $e(t)$	cr
	50	4.21e-2		5.45e-2		1.17e-2		8.35e-3	
	100	3.08e-2	0.453	4.43e-2	0.298	6.15e-3	0.924	7.34e-3	0.187
	150	2.56e-2	0.456	3.83e-2	0.358	5.17e-3	0.429	8.21e-3	−0.277
0.105	200	2.23e-2	0.478	3.44e-2	0.371	5.14e-3	0.020	8.65e-3	−0.184
	300	1.63e-2	0.776	2.86e-2	0.457	4.83e-3	0.153	7.87e-3	0.234
	400	1.44e-2	0.459	2.60e-2	0.341	5.20e-3	−0.258	7.36e-3	0.230
	600	1.10e-2	0.649	2.25e-2	0.354	4.91e-3	0.145	6.34e-3	0.369
	800	9.16e-3	0.622	2.06e-2	0.311	4.80e-3	0.074	5.86e-3	0.277
	50	1.01e-1		1.27e-1		4.54e-2		5.12e-2	
	100	7.53e-2	0.428	1.08e-1	0.229	2.60e-2	0.805	3.23e-2	0.662
	150	6.25e-2	0.459	1.04e-1	0.103	1.88e-2	0.792	2.27e-2	0.869
0.35	200	5.47e-2	0.462	1.01e-1	0.080	1.42e-2	0.985	1.82e-2	0.772
	300	4.63e-2	0.416	9.67e-2	0.119	9.69e-3	0.943	1.35e-2	0.744
	400	4.22e-2	0.320	9.18e-2	0.180	7.36e-3	0.955	1.15e-2	0.558
	600	3.90e-2	0.192	8.57e-2	0.170	5.33e-3	0.795	9.31e-3	0.514
	800	3.74e-2	0.150	8.08e-2	0.203	4.90e-3	0.296	8.03e-3	0.516
	50	1.51e-1		1.64e-1		2.99e-2		4.57e-2	
	100	1.09e-1	0.472	1.36e-1	0.271	1.68e-2	0.832	2.55e-2	0.843
	150	9.37e-2	0.373	1.31e-1	0.094	1.23e-2	0.773	1.88e-2	0.752
0.84	200	8.64e-2	0.284	1.30e-1	0.025	9.88e-3	0.758	1.52e-2	0.730
	300	7.73e-2	0.274	1.29e-1	0.020	7.47e-3	0.688	1.15e-2	0.697
	400	7.13e-2	0.279	1.27e-1	0.063	6.18e-3	0.661	9.46e-3	0.671
	600	6.18e-2	0.353	1.21e-1	0.118	4.88e-3	0.582	7.36e-3	0.620
	800	5.44e-2	0.442	1.14e-1	0.204	4.19e-3	0.526	6.21e-3	0.593
	50	3.73e-2		5.25e-2		5.02e-3		1.44e-2	
	100	2.54e-2	0.550	4.85e-2	0.114	2.46e-3	1.03	9.11e-3	0.665
	150	1.95e-2	0.660	4.80e-2	0.029	1.61e-3	1.04	6.40e-3	0.872
3.5	200	1.61e-2	0.663	4.64e-2	0.117	1.19e-3	1.05	5.06e-3	0.813
	300	1.25e-2	0.615	4.32e-2	0.176	7.79e-4	1.05	3.62e-3	0.826
	400	1.06e-2	0.587	4.08e-2	0.201	5.75e-4	1.06	2.86e-3	0.825
	600	8.37e-3	0.581	3.78e-2	0.190	3.71e-4	1.08	2.04e-3	0.826
	800	7.06e-3	0.593	3.60e-2	0.164	2.70e-4	1.11	1.61e-3	0.824

Table 1 displays the errors $e(t)$ for the four schemes KT2A, KT2B, LxFA and LxFB at four different times. We find confirmed that for a given scheme and discretization, the error varies drastically during computation and is large for those times where the exact solution exhibits strong shocks. Moreover, as expected, the errors for the LxFA and LxFB schemes are much larger than for the KT schemes. Except for the time $t = 0.105$, the convergence rates for the KT schemes are larger than for the LxF schemes.

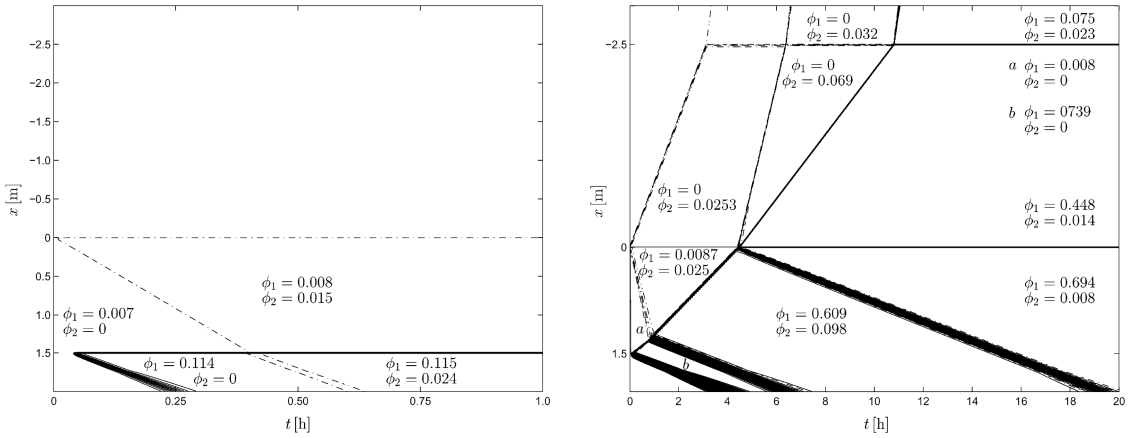

Fig. 6. Example 2 (left) and Example 3 (right): Simulation of a continuous separation of a bidisperse equal-density suspension of larger (Species 1, solid) and smaller (Species 2, dashdotted) particles according to Spannenberg et al. [68]. The iso-concentration lines correspond to $\phi_1, \phi_2 = 0, 0.005, 0.001, \ldots, 0.995, 1$.

4.2. Application to a hyperbolic system of conservation laws

Spannenberg et al. [68] report an experiment of continuous sedimentation of a bidisperse suspension in a clarifier-thickener. The spherical ballotini particles are of the same material having density $\varrho_s = 2370\ \mathrm{kg/m^3}$ and differ in size with $d_1 = 2.56 \times 10^{-4}$ m and $d_2 = 5.8 \times 10^{-5}$ m, and thus $\delta_2 = 0.05133$. In this equal-density case, the MLB model leads to a strictly hyperbolic 2×2 system, as discussed in Section 2.3.

To explain their experimental findings, Spannenberg et al. suggested the model of Lockett and Al-Habbooby [51,52], which also involves a Richardson–Zaki-type hindered settling factor (2.5), for which the exponent $n = 4.65$ was found to be suitable. It is, however, well known that the Lockett and Al-Habbooby model is algebraically simple but unrealistic [8,54], and we therefore use the same hindered settling factor with the MLB model.

The fluid parameters are $\varrho_f = 1110\ \mathrm{kg/m^3}$ and $\mu_f = 4.7 \times 10^{-3}$ Pa s. These and $g = 9.81\ \mathrm{m/s^2}$ imply $\bar{\varrho}_s = 1260\ \mathrm{kg/m^3}$ and $\mu = 7.5994 \times 10^{-6}\ \mathrm{m^4/(kg\,s)}$. The experimental equipment is a column of height 4 m, with the feed source being located 1.5 m above the underflow level. Thus, if x denotes the depth measured in meters, we consider the interval $[-2.5, 1.5]$ (instead of $[-1, 1]$).

We consider here two cases (Examples 2 and 3), both starting from a vessel full of water ($\phi_1^0 = \phi_2^0 = 0$), see Fig. 6. In the first (Example 2), we adopt the control variables $q_R = 6.333 \times 10^{-4}$ m/s, $q_L = -6.005 \times 10^{-5}$ m/s, $\phi_1^F = 0.1049$ and $\phi_2^F = 0.0221$ used by Spannenberg et al. [68] (and expressed in new units) in their (unique) experiment. In the second (Example 3) we basically apply the same parameters except that we choose $q_R = 0.333 \times 10^{-4}$ m/s and $q_L = -6.602 \times 10^{-4}$ m/s. In both cases we have $q_R - q_L = 6.9335 \times 10^{-4}$ m/s. Consequently, Example 3 illustrates what would have happened if the experimentators had repeated the experiment (Example 2) maintaining same the feed rate and composition but reducing the discharge flow rate. In the case of Example 3, material immediately enters both the clarification and thickening zones, accumulates at the bottom and forms a rising sediment, which eventually breaks through the feed level, as in Example 1. We observe that the solution is remarkably complicated with eleven areas of constant composition. The main difference

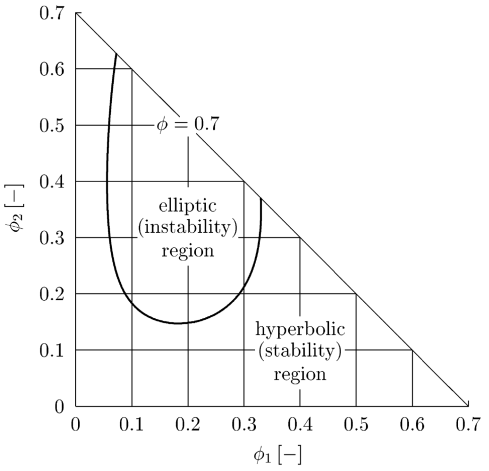

Fig. 7. Elliptic (instability) region of the MLB model for a bidisperse suspension with $n = 5.765$, $\delta_1 = 0.1234$ and $\bar{\varrho}_1/\bar{\varrho}_2 = -0.04046$ [57].

to Example 1 is that when the rising shock representing the sediment level reaches the feed level, new kinematic shocks traveling both upwards and downwards are created.

In Example 2 we choose $J = 500$, $\lambda = 10$, whereas in Example 3 we choose $J = 800$, $\lambda = 8.0$.

4.3. Application to a hyperbolic-elliptic system of conservation laws

We now simulate the continuous separation of a bidisperse suspension ($N = 2$) in the continuous clarifier-thickener described in Section 2.4. In their papers, Nasr-El-Din et al. [56–58] exclusively consider bidisperse suspensions with one buoyant (lighter than the fluid) and one heavy (heavier than the fluid) species, and we here closely adapt the parameters of the experimental results described in [57] (see Fig. 7). In the framework of the MLB model, such heavy-buoyant systems usually lead to hyperbolic-elliptic mixed type equations. We show here that our numerical scheme also yields reasonable results for this case.

Nasr-El-Din et al. [57] consider a bidisperse suspension of polysterene particles ($d_1 = 3.9 \times 10^{-4}$ m, $\varrho_1 = 1050$ kg/m^3) and glass beads ($d_2 = 1.37 \times 10^{-4}$ m, $\varrho_2 = 2850$ kg/m^3) suspended in a salt solution ($\varrho_f = 1120$ kg/m^3, $\mu_f = 1.41 \times 10^{-3}$ Pa s). For monodisperse suspensions of each particle species, the flux function (2.16) was found to be suitable with the exponents $n = n_1 = 5.705$ and $n = n_2 = 5.826$, respectively. The remaining parameters are $\delta_2 = (d_2/d_1)^2 = 0.1234$, $\bar{\varrho}_1 = -70$ kg/m^3, $\bar{\varrho}_2 = 1730$ kg/m^3 and $\mu = 5.879 \times 10^{-5}$m^4/(kg s). For polydisperse calculations we here utilize the hindered settling function defined by (2.5) with $\phi_{\max} = 0.7$ and $n = (n_1 + n_2)/2 = 5.765$.

The equipment used in [57] is a cylindrical clarifier-thickener of total height 40 cm with the feed source located in the middle, and a rectangular cross-sectional area $S = 4.24 \times 10^{-4}$ m^2. Nasr-El-Din et al. [57] report experiments with many different feed and discharge fluxes. We consider here just two of the cases of continuous sedimentation reported (our Examples 4 and 5), and present a simulation of one hypothetical additional experiment (Example 6).

Example 4 corresponds to a volume feed flux of $Q_F = 13.2$ cm^3/s according to [57], of which 75% are directed into the thickening and 25% into the clarification zone, which implies $q_R = 2.3349 \times$

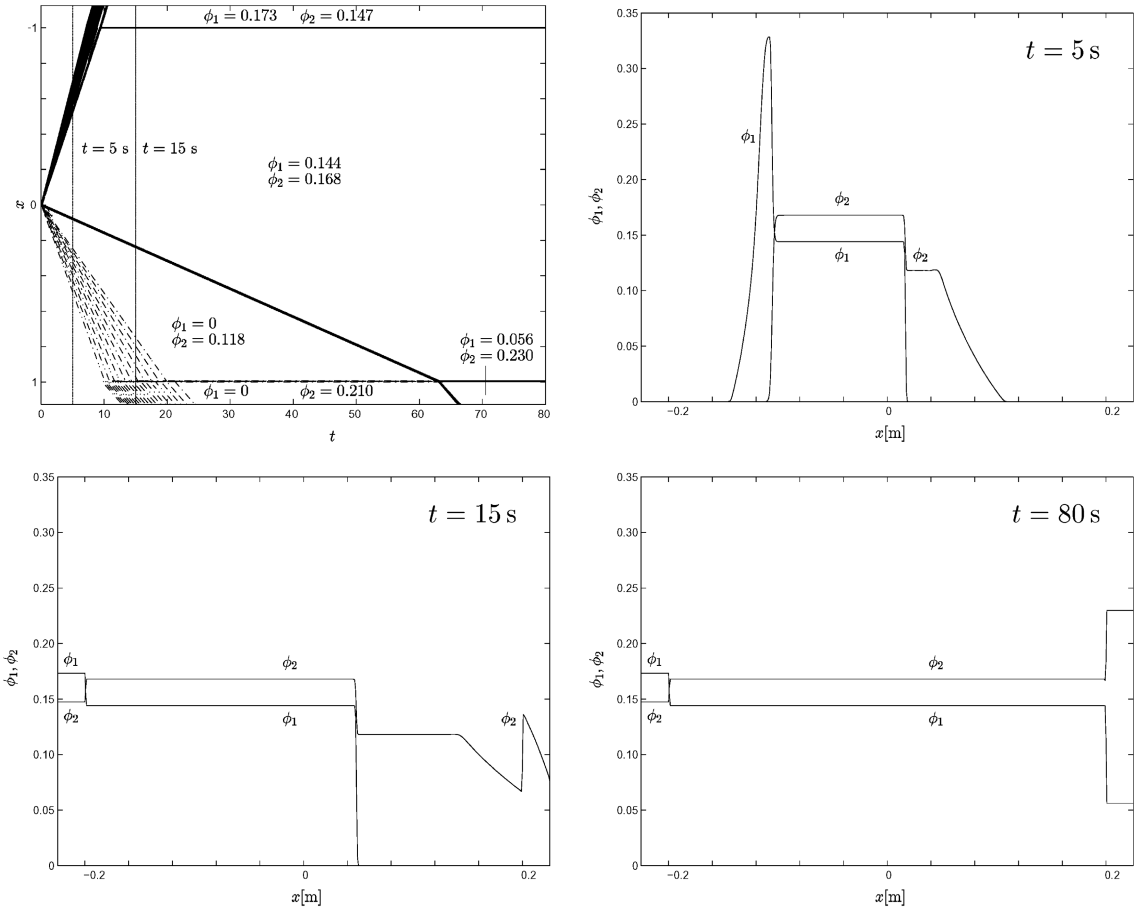

Fig. 8. Example 4: Simulation of continuous separation of a bidisperse suspension of buoyant (Species 1) and heavy (Species 2) particles with $\phi_1^{\mathrm{F}} = 0.144$ and $\phi_2^{\mathrm{F}} = 0.168$. Top left: iso-concentration lines (solid: Species 1, dashdotted: Species 2; for the values $0, 0.01, 0.02, \ldots$) and areas of constant composition, top right and bottom: concentration profiles at three selected times.

10^{-2} m/s and $q_{\mathrm{L}} = -7.783 \times 10^{-3}$ m/s. The feed concentrations are $\phi_1^{\mathrm{F}} = 0.144$ and $\phi_2^{\mathrm{F}} = 0.168$. Example 5 is a variant of this case, also considered in [57], with $Q_{\mathrm{F}} = 4.4\ \mathrm{cm}^3/\mathrm{s}$, the same 'split ratio' 75%, i.e. $q_{\mathrm{R}} = 7.783 \times 10^{-3}$ m/s and $q_{\mathrm{L}} = -2.594 \times 10^{-3}$ m/s. The feed concentrations are $\phi_1^{\mathrm{F}} = 0.065$ and $\phi_2^{\mathrm{F}} = 0.067$. Figs. 8 and 9 show numerical simulations of these cases produced by the KTA2 scheme with $\Delta x = 0.4/J$, $J = 500$, and $\lambda = 10$. In both cases, a stationary solution is assumed; in Example 4 (Fig. 8), a steady flow establishes in which the overflow contains both species at similar compositions and the heavy Species 2 is clearly dominant in the underflow, while in Example 5, Species 2 does not enter the clarification zone. Moreover, we observe in Example 4 the formation of a region where the concentrations are $\phi_1 = 0.144$ and $\phi_2 = 0.168$ in the interior of the equipment. These values are identical to the feed concentration and cause the equations to be elliptic. Since according to our discussion in Section 2.3, (local) ellipticity is a criterion for the occurrence of instabilities, our result is consistent with the qualified statement by Nasr-El-Din

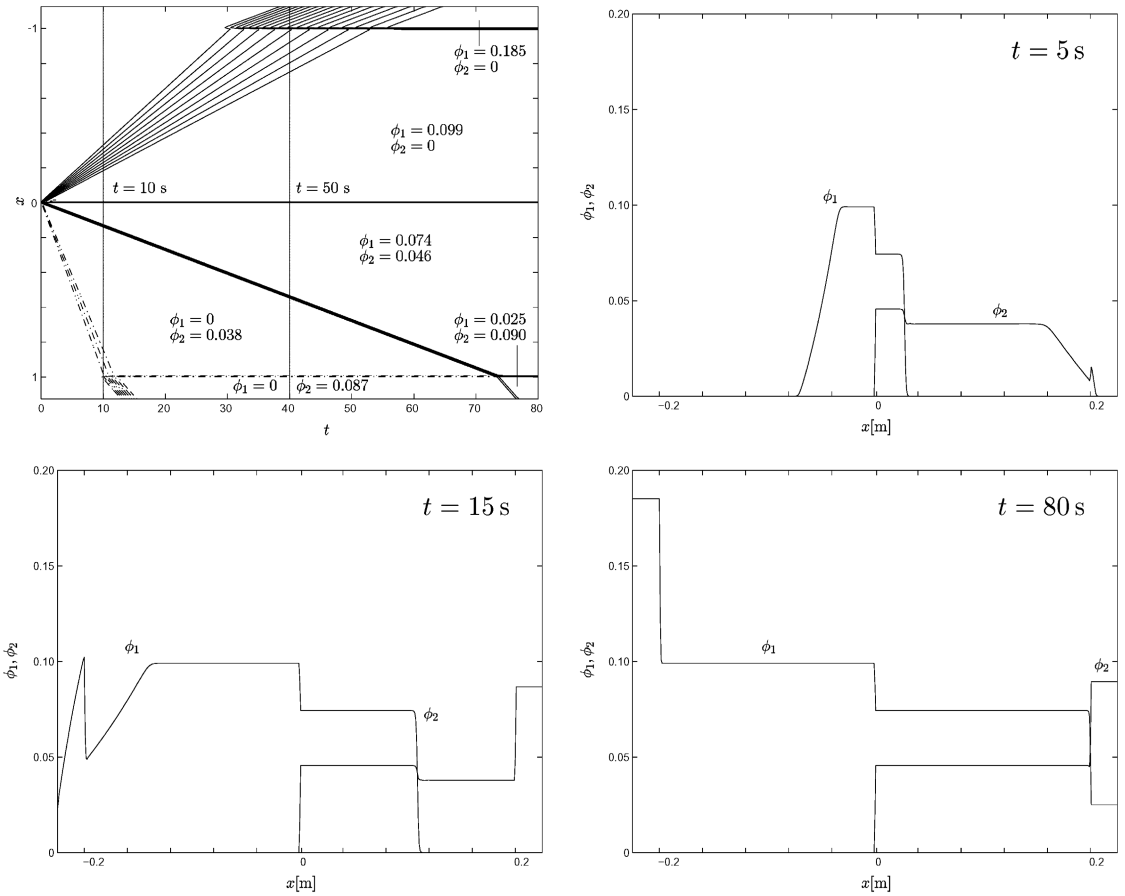

Fig. 9. Example 5: Simulation of continuous separation of a bidisperse suspension of buoyant (Species 1) and heavy (Species 2) particles with $\phi_1^F = 0.065$ and $\phi_2^F = 0.067$. Top left: iso-concentration lines and areas of constant composition, top right and bottom: concentration profiles at three selected times.

et al. [57, p. 1010] that for these flow parameters, "flow visualization studies indicated that the local instability extends to the whole length of the settler". No ellipticity region appears in the numerical simulation of Example 5 (Fig. 9), and for that case no instabilities were observed experimentally [57, p. 1007].

Example 6 represents a hypothetical experiment. We consider a closed settling column with no feed or discharge (i.e., $q_L = q_R = 0$) and assume that initially the upper half is filled with suspension consisting only of heavy particles and the lower half filled with suspension containing only light particles; more specifically, we select

$$\phi_1^0 = \begin{cases} 0.18 & \text{for } 0 \leqslant x \leqslant 0.2, \\ 0 & \text{for } 0.2 < x \leqslant 0.4, \end{cases} \qquad \phi_2^0 = \begin{cases} 0 & \text{for } 0 \leqslant x \leqslant 0.2, \\ 0.18 & \text{for } 0.2 < x \leqslant 0.4. \end{cases} \tag{4.1}$$

The interesting features of the solution appear near $x = 0.2$, and are unaffected by the boundaries $x = 0$ and $x = 0.4$. Thus we regard this case as a Riemann problem. Clearly, the equations are hyperbolic

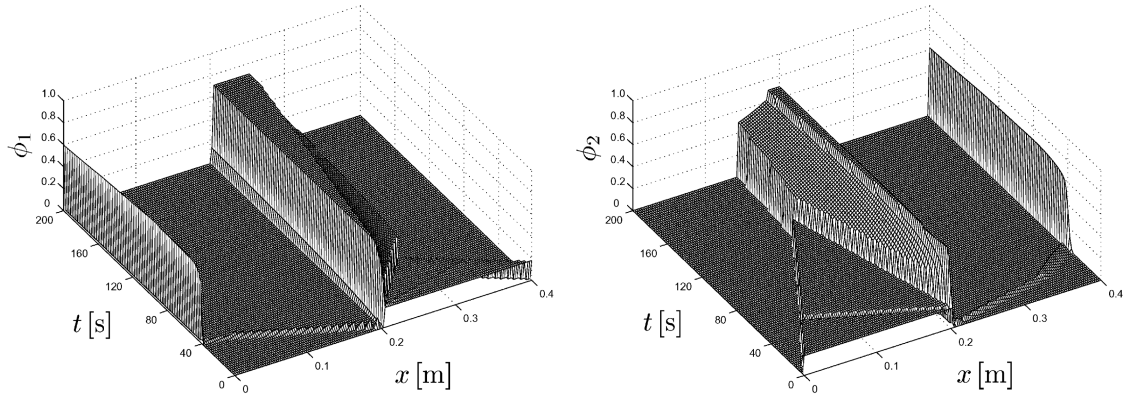

Fig. 10. Example 6: Solution of a Riemann problem with the heavy particles initially located above the light.

on the line $t = 0$, but the state $(0.18, 0.18)$ causes the equations to be elliptic. Similar heavy-buoyant configurations, with the main idea being that the trajectories of the upwards and downwards moving particles should cross each other, have been studied experimentally by Law et al. [46] and were simulated in our previous paper [8]. We have simulated this separation with very high accuracy (the interval $[0, 0.4]$ was subdivided into $J = 5000$ cells) and obtained the result shown in Fig. 10.

According to this simulation, only a very small amount of the light particles (Species 1) passes through the layer of heavy particles and arrives at the top end of the column $x=0$ to form a sediment there, and vice versa. After very short time, both species "lock" each other at $x=0$, which means that both the upwards motion of light particles and the downwards motion of heavy particles is stopped, and we observe the formation of sediment "onto" $x = 0$ from both sides. This anomalous solution was not observed in experiments and the numerical simulations in [8]. We have strong reason to believe that the unusual nature of this solution is related to the ellipticity region. In fact, it turned out that near $x = 0$ and for small times, a small region in the x-t-plane forms where the equation assumes elliptic type, and which could be responsible for the locking effect. The formation of this ellipticity region in the x-t-plane seems to be related to the choice of the adjacent concentrations in (4.1); for example, $(0.18, 0.18)$ is a state that clearly belongs to the ellipticity region drawn in Fig. 7, and we calculated the same example with 0.18 replaced by some smaller value u_0. The solution qualitatively was the same as in Fig. 10 whenever (u_0, u_0) fell into the ellipticity region; otherwise solutions looked similar to those of [8]. These vague remarks should emphasize that the analysis of hyperbolic-elliptic systems in the present model is far from being well understood, although it has been clearly shown [16] that these mixed-type equations are physically appropriate. For similar reasons, there is at present no guarantee that numerical schemes converge to physically meaningful solutions.

5. Conclusions

The mathematical model of continuous sedimentation of polydisperse sedimentation derived herein is a straightforward combination of previous works on continuous sedimentation of monodisperse

suspensions and batch settling of polydisperse suspensions. The term "clarifier-thickener" is utilized herein in order to be consistent with previous analyzes of the monodisperse case [10–15]. However, unlike the monodisperse case, the focus in applications of the present model will not primarily be on thickening of a given suspension. Rather, practitioners are interested in separating well mixed polydisperse suspensions in order to recover the different particle species in monodisperse suspensions ("products"). This operation is known as classification. Obviously, a clarifier-thickener can produce only two products simultaneously. For more products, the one-dimensional clarifier-thickener setup can be extended to a simple hydrodynamic model of classification into N products if additional sinks, permitting to "tap" the equipment at different heights, are provided. Several engineering papers suggest such models [1,26,60]. However, sink terms are more difficult to include than source terms, since the composition of the tapped mixture is unknown and therefore part of the solution, while the composition of feed suspension injected into the unit can be prescribed. We will come back to the treatment of sink terms in a forthcoming paper.

A natural question arising from our model is that of agreement with experimental data. Some of the numerical examples presented herein are based on experimental information. The numerical results qualitatively agree with the published experimental information. The problem is that the model predicts the detailed dynamics of the separation in the interior of the unit, while most experimental data, for example those recorded in [56–58], are related to the composition of the overflow and underflow at steady state and general observations of instability only. Similarly, in [68] only the underflow flux of each species and one concentration profile of the smaller species are shown. The difficulty is with measuring individual particle species concentrations in a polydisperse, continuously operated system. For the batch settling in a closed column, some systematic experiments to evaluate the predictions of several polydisperse sedimentation models have been conducted, see [46,64].

Continuing our previous work [8,9], we have here devised first- and second-order accurate numerical schemes of central type [44,59,69] for systems of conservation laws like (1.1) containing discontinuous coefficients. We derived central schemes by discretizing the enlarged system (1.3) (not the original system (1.1)) in which the discontinuous coefficients are treated as additional conservation laws (1.2). The additional conservation laws (1.2) were then discretized (solved approximately) or solved exactly, giving raise to different classes of numerical schemes. Our motivation for considering the enlarged system (1.3) comes from the mathematical treatment of equations with discontinuous coefficients, see, e.g., [27,28,33] and the other references cited in Section 1. Discretizing the enlarged system would be consistent with adding artificial viscosity to both (1.1) and (1.2) in the continuous case, an approach taken in, e.g., [27] to solve the Riemann problem for a scalar conservation law with a discontinuous coefficient. Our motivation for building numerical schemes based on the exact evolution of the discontinuous coefficients comes from the scalar convergence theory developed in [40,71,72]. The general conclusion is that the second-order central schemes (based on both the approximate and exact evolution of the coefficients) generate satisfactory results, and, at the same time, they are easy to implement. We also add that the schemes based on the exact solution of the conservation laws for the discontinuous coefficients are more accurate than those based on the approximate solution of these laws. A convergence result for the Lax–Friedrichs scheme (based on the exact evolution of the discontinuous coefficients) for a scalar conservation law with a discontinuous coefficient can be found in [40].

The use of central difference schemes for the simulation of polydisperse sedimentation in closed columns was introduced in [8,9] and has meanwhile been adopted by Xue and Sun [73]. We have

illustrated here that the semi-discrete version of the KT scheme, which is also the one chosen in [73], can be employed to accurately simulate continuous sedimentation in the presence of source terms, while the fully discrete KT scheme utilized in [9] leads to oscillatory solutions. Moreover, the semi-discrete scheme also produces physically reasonable looking results in the hyperbolic-elliptic examples. However, it is at present very difficult to evaluate the quality of these solutions, since virtually all mathematical questions and physical insight in the hyperbolic-elliptic case are still unresolved.

Acknowledgements

This work has been supported by the Collaborative Research Center (Sonderforschungsbereich) 404 at the University of Stuttgart and (in part) by the BeMatA program of the Research Council of Norway.

References

[1] L.G. Austin, C.H. Lee, F. Concha, P.T. Luckie, Hindered settling and classification partition curves, Miner. Metall. Process. 9 (1992) 161–168.
[2] D.S. Bale, R.J. LeVeque, S. Mitran, J.A. Rossmanith, A wave propagation method for conservation laws and balance laws with spatially varying flux functions, SIAM J. Sci. Comp. 24 (2002) 955–978.
[3] N.G. Barton, C.-H. Li, S.J. Spencer, Control of a surface of discontinuity in continuous thickeners, J. Austral. Math. Soc. Ser. B 33 (1992) 269–289.
[4] G.K. Batchelor, R.W. Janse van Rensburg, Sedimentation in a dilute polydisperse system of interacting spheres, J. Fluid Mech. 119 (1982) 379–408.
[5] S. Berres, R. Bürger, On gravity and centrifugal separation of polydisperse suspensions forming compressible sediments, Internat. J. Solids Structures (2003), to appear.
[6] S. Berres, R. Bürger, K.H. Karlsen, E.M. Tory, Strongly degenerate parabolic-hyperbolic systems modeling polydisperse sedimentation with compression, SIAM J. Appl. Math., to appear.
[7] F. Bouchut, F. James, One-dimensional transport equations with discontinuous coefficients, Nonlinear Anal. TMA 32 (1998) 891–933.
[8] R. Bürger, F. Concha, K.-K. Fjelde, K.H. Karlsen, Numerical simulation of the settling of polydisperse suspensions of spheres, Powder Technol. 113 (2000) 30–54.
[9] R. Bürger, K.-K. Fjelde, K. Höfler, K.H. Karlsen, Central difference solutions of the kinematic model of settling of polydisperse suspensions and three-dimensional particle-scale simulations, J. Eng. Math. 41 (2001) 167–187.
[10] R. Bürger, K.H. Karlsen, C. Klingenberg, N.H. Risebro, A front tracking approach to a model of continuous sedimentation in ideal clarifier-thickener units, Nonlinear Anal. Real World Appl. 4 (2003) 457–481.
[11] R. Bürger, K.H. Karlsen, N.H. Risebro, A relaxation scheme for continuous sedimentation in ideal clarifier-thickener units, Comput. Math. Appl., submitted.
[12] R. Bürger, K.H. Karlsen, N.H. Risebro, J.D. Towers, Numerical methods for the simulation of continuous sedimentation in ideal clarifier-thickener units, Internat. J. Mineral Process., to appear.
[13] R. Bürger, K.H. Karlsen, N.H. Risebro, J.D. Towers, Monotone difference approximations for the simulation of clarifier-thickener units, Comput. Visual. Sci., to appear.
[14] R. Bürger, K.H. Karlsen, N.H. Risebro, J.D. Towers, On a model for continuous sedimentation in vessels with discontinuously varying cross-sectional area, In: T.Y. Hou, E. Tadmor (Eds.), Hyperbolic Problems: Theory, Numerics, Applications, Springer-Verlag, to appear.
[15] R. Bürger, K.H. Karlsen, N.H. Risebro, J.D. Towers, Well-posedness in BV_t and convergence of a difference scheme for continuous sedimentation in ideal clarifier-thickener units, Preprint 2003/18, Sonderforschungsbereich 404, University of Stuttgart, 2003.

[16] R. Bürger, K.H. Karlsen, E.M. Tory, W.L. Wendland, Model equations and instability regions for the sedimentation of polydisperse suspensions of spheres, Z. Angew. Math. Mech. 82 (2002) 699–722.
[17] R. Bürger, W.L. Wendland, F. Concha, Model equations for gravitational sedimentation-consolidation processes, Z. Angew. Math. Mech. 80 (2000) 79–92.
[18] S. Čanić, Blood flow through compliant vessels after endovascular repair: well deformations induced by the discontinuous wall properties, Comput. Visual. Sci. 4 (2002) 147–155.
[19] J.P. Chancelier, M. Cohen de Lara, F. Pacard, Analysis of a conservation PDE with discontinuous flux: a model of settler, SIAM J. Appl. Math. 54 (1994) 954–995.
[20] F. Concha, A. Barrientos, M.C. Bustos, Phenomenological model of high capacity thickening, in: Proceedings of the 19th International Minerals Processing Congress (XIX IMPC), San Francisco, USA, pp. 75–79 (Chapter 14).
[21] S. Diehl, On scalar conservation laws with point source and discontinuous flux function, SIAM J. Math. Anal. 26 (1995) 1425–1451.
[22] S. Diehl, A conservation law with point source and discontinuous flux function modelling continuous sedimentation, SIAM J. Appl. Math. 56 (1996) 388–419.
[23] S. Diehl, Dynamic and steady-state behaviour of continuous sedimentation, SIAM J. Appl. Math. 57 (1997) 991–1018.
[24] S. Diehl, On boundary conditions and solutions for ideal clarifier-thickener units, Chem. Eng. J. 80 (2000) 119–133.
[25] S. Diehl, Operating charts for continuous sedimentation I: control of steady states, J. Eng. Math. 41 (2001) 117–144.
[26] K.P. Galvin, E. Doroodchi, A.M. Callen, N. Lambert, S.J. Pratten, Pilot plant trial of the reflux classifier, Miner. Eng. 15 (2002) 19–25.
[27] T. Gimse, N.H. Risebro, Riemann problems with a discontinuous flux function, Third International Conference on Hyperbolic Problems, Vol. I, II (Uppsala, 1990), Studentlitteratur, Lund, 1991, pp. 488–502.
[28] T. Gimse, N.H. Risebro, Solution of the Cauchy problem for a conservation law with a discontinuous flux function, SIAM J. Math. Anal. 23 (1992) 635–648.
[29] L. Gosse, F. James, Numerical approximations of one-dimensional linear conservation equations with discontinuous coefficients, Math. Comput. 69 (2000) 987–1015.
[30] J.M. Greenberg, A.Y. Le Roux, A well-balanced scheme for the numerical processing of source terms in hyperbolic equations, SIAM J. Numer. Anal. 33 (1996) 1–16.
[31] H. Holden, N.H. Risebro, A mathematical model of traffic flow on a network of unidirectional roads, SIAM J. Math. Anal. 26 (1995) 999–1017.
[32] J.M.-K. Hong, Part I: An extension of the Riemann problems and Glimm's method to general systems of conservation laws with source terms, Part II: A total variation bound on the conserved quantities for a generic resonant nonlinear balance laws, Ph.D. Thesis, University of California, Davis, 2000.
[33] E. Isaacson, B. Temple, Nonlinear resonance in systems of conservation laws, SIAM J. Appl. Math. 52 (1992) 1260–1278.
[34] E. Isaacson, B. Temple, Convergence of the 2×2 Godunov method for a general resonant nonlinear balance law, SIAM J. Appl. Math. 55 (1995) 625–640.
[35] K.H. Karlsen, C. Klingenberg, N.H. Risebro, A relaxation scheme for conservation laws with discontinuous coefficients, Math. Comp., to appear.
[36] K.H. Karlsen, N.H. Risebro, Unconditionally stable methods for Hamilton-Jacobi equations, J. Comput. Phys. 180 (2002) 710–735.
[37] K.H. Karlsen, N.H. Risebro, J.D. Towers, L^1 stability for entropy solutions of degenerate parabolic convection-diffusion equations with discontinuous coefficients, Preprint, 2003, Available at the URL http://www.math.ntnu.no/conservation/.
[38] K.H. Karlsen, N.H. Risebro, J.D. Towers, On a nonlinear degenerate parabolic transport-diffusion equation with a discontinuous coefficient, Electron. J. Differential Equations 2002 (93) (2002) 1–23.
[39] K.H. Karlsen, N.H. Risebro, J.D. Towers, Upwind difference approximations for degenerate parabolic convection-diffusion equations with a discontinuous coefficient, IMA J. Numer. Anal. 22 (2002) 623–664.
[40] K.H. Karlsen, N.H. Risebro, J.D. Towers, Convergence of the Lax-Friedrichs scheme for conservation laws with a discontinuous coefficient, in preparation.

[41] R.A. Klausen, N.H. Risebro, Stability of conservation laws with discontinuous coefficients, J. Differential Equations 157 (1999) 41–60.
[42] C. Klingenberg, N.H. Risebro, Convex conservation laws with discontinuous coefficients. Existence, uniqueness and asymptotic behavior, Commun. Partial Differential Equations 20 (1995) 1959–1990.
[43] C. Klingenberg, N.H. Risebro, Stability of a resonant system of conservation laws modeling polymer flow with gravitation, J. Differential Equations 170 (2001) 344–380.
[44] A. Kurganov, E. Tadmor, New high-resolution central schemes for nonlinear conservation laws and convection-diffusion equations, J. Comput. Phys. 160 (2000) 241–282.
[45] G.J. Kynch, A theory of sedimentation, Trans. Faraday Soc. 48 (1952) 166–176.
[46] H.-S. Law, J.H. Masliyah, R.S. MacTaggart, K. Nandakumar, Gravity separation of bidisperse suspensions: light and heavy particle species, Chem. Eng. Sci. 42 (1987) 1527–1538.
[47] O. Lev, E. Rubin, M. Sheintuch, Steady state analysis of a continuous clarifier-thickener system, A.I.Ch.E J. 32 (1986) 1516–1525.
[48] L.W. Lin, B. Temple, J.H. Wang, A comparison of convergence rates for Godunov's method and Glimm's method in resonant nonlinear systems of conservation laws, SIAM J. Numer. Anal. 32 (1995) 824–840.
[49] L.W. Lin, B. Temple, J.H. Wang, Suppression of oscillations in Godunov's method for a resonant non-strictly hyperbolic system, SIAM J. Numer. Anal. 32 (1995) 841–864.
[50] T.P. Liu, Resonance for a quasilinear hyperbolic equation, J. Math. Phys. 28 (1987) 2593–2602.
[51] M.J. Lockett, H.M. Al-Habbooby, Differential settling by size of two particles in a liquid, Trans. Inst. Chem. Eng. 51 (1973) 281–292.
[52] M.J. Lockett, H.M. Al-Habbooby, Relative particle velocities in two-species settling, Powder Technol. 10 (1974) 67–71.
[53] M.J. Lockett, K.S. Bassoon, Sedimentation of binary particle mixtures, Powder Technol. 24 (1979) 1–7.
[54] J.H. Masliyah, Hindered settling in a multiple-species particle system, Chem. Eng. Sci. 34 (1979) 1166–1168.
[55] S. Mochon, An analysis of the traffic on highways with changing surface conditions, Math. Modelling 9 (1987) 1–11.
[56] H. Nasr-El-Din, J.H. Masliyah, K. Nandakumar, Continuous gravity separation of concentrated bidisperse suspensions in a vertical column, Chem. Eng. Sci. 45 (1990) 849–857.
[57] H. Nasr-El-Din, J.H. Masliyah, K. Nandakumar, Continuous separation of suspensions containing light and heavy particle species, Canad. J. Chem. Eng. 77 (1999) 1003–1012.
[58] H. Nasr-El-Din, J.H. Masliyah, K. Nandakumar, D.H.-S. Law, Continuous gravity separation of a bidisperse suspension in a vertical column, Chem. Eng. Sci. 43 (1988) 3225–3234.
[59] H. Nessyahu, E. Tadmor, Non-oscillatory central differencing for hyperbolic conservation laws, J. Comput. Phys. 87 (1990) 408–463.
[60] G. Nguyentranlam, K.P. Galvin, Particle classification in the reflux classifier, Miner. Eng. 14 (2001) 1081–1091.
[61] D.N. Ostrov, Viscosity solutions and convergence of monotone schemes for synthetic aperture radar shape-from-shading equations with discontinuous intensities, SIAM J. Appl. Math. 59 (1999) 2060–2085.
[62] D.N. Ostrov, Extending viscosity solutions to Eikonal equations with discontinuous spatial dependence, Nonlinear. Anal. TMA 42 (2000) 709–736.
[63] D.N. Ostrov, Solutions of Hamilton-Jacobi equations and scalar conservation laws with discontinuous space-time dependence, J. Differential Equations 182 (2002) 51–77.
[64] V.S. Patwardhan, C. Tien, Sedimentation and liquid fluidization of solid particles of different sizes and densities, Chem. Eng. Sci. 40 (1985) 1051–1060.
[65] G. Petrova, B. Popov, Linear transport equations with discontinuous coefficients, Commun. Partial Differential Equations 24 (1999) 1849–1873.
[66] J.F. Richardson, W.N. Zaki, Sedimentation and fluidization: Part I, Trans. Inst. Chem. Eng. 32 (1954) 35–53.
[67] N. Seguin, J. Vovelle, Analysis and approximation of a scalar conservation law with a flux function with discontinuous coefficients, Preprint, 2002.
[68] A. Spannenberg, K. Galvin, J. Raven, M. Scarboro, Continuous differential sedimentation of a binary suspension, Chem. Eng. in Austral. 21 (1996) 7–11.
[69] E. Tadmor, Approximate solutions of nonlinear conservation laws, in: A. Quarteroni (Ed.), Lecture Notes in Mathematics 1697, 1997 C.I.M.E. Course in Cetraro, Italy, June 1997, Springer, Berlin, 1998, pp. 1–149.

[70] B. Temple, Global solution of the Cauchy problem for a class of 2×2 nonstrictly hyperbolic conservation laws, Adv. Appl. Math. 3 (1982) 335–375.
[71] J.D. Towers, Convergence of a difference scheme for conservation laws with a discontinuous flux, SIAM J. Numer. Anal. 38 (2000) 681–698.
[72] J.D. Towers, A difference scheme for conservation laws with a discontinuous flux: the nonconvex case, SIAM J. Numer. Anal. 39 (2001) 1197–1218.
[73] B. Xue, Y. Sun, Modeling of sedimentation of polydisperse spherical beads with a broad size distribution, Chem. Eng. Sci. 58 (2003) 1531–1543.